

# Positive cross-correlations due to Dynamical Channel-Blockade in a three-terminal quantum dot

A. Cottet, W. Belzig, and C. Bruder

Department of Physics and Astronomy, University of Basel, Klingelbergstrasse 82, 4056 Basel, Switzerland  
(Dated: March 22, 2024)

We investigate current fluctuations in a three-terminal quantum dot in the sequential tunneling regime. In the voltage-bias configuration chosen here, the circuit is operated like a beam splitter, i.e. one lead is used as an input and the other two as outputs. In the limit where a double occupancy of the dot is not possible, a super-Poissonian Fano factor of the current in the input lead and positive cross-correlations between the current fluctuations in the two output leads can be obtained, due to dynamical channel-blockade. When a single orbital of the dot transports current, this effect can be obtained by lifting the spin-degeneracy of the circuit with ferromagnetic leads or with a magnetic field. When several orbitals participate in the electronic conduction, lifting spin-degeneracy is not necessary. In all cases, we show that a super-Poissonian Fano factor for the input current is not equivalent to positive cross-correlations between the outputs. We identify the conditions for obtaining these two effects and discuss possible experimental realizations.

PACS numbers: 73.23.-b, 72.70.+m, 72.25.Rb

## I. INTRODUCTION

The study of current noise in mesoscopic circuits has become a central subfield of mesoscopic physics because it allows to access informations not available through measurements of the average currents (for reviews, see Refs. [1, 2]). Current fluctuations can first be probed through the auto-correlations of the current fluctuations in one branch of the circuit. For conductors with open channels, the fermionic statistics of electrons result in a suppression of these auto-correlations below the Poisson limit [3, 4, 5]. In a multi-terminal circuit, current fluctuations can also be probed through the cross-correlations between two different branches. Buttiker has shown that in a non-interacting electronic circuit, the zero-frequency current cross-correlations are always negative provided the leads of the circuit are thermal reservoirs maintained at constant voltage-potentials [6]. On the experimental side, negative cross-correlations have been measured very recently by Henny et al. [7] and Oliver et al. [8] in mesoscopic beam splitters. Oberholzer et al. have shown how the cross-correlations vanish in the classical limit [9].

Up to now, positive cross-correlations have never been measured in electronic circuits. However, nothing forbids to reverse the sign of cross-correlations if a hypothesis of Buttiker's proof is not fulfilled (see Ref. [10] for a recent review). First, it has been shown theoretically that positive cross-correlations can be obtained in an electronic circuit by relaxing the hypotheses of Buttiker regarding the leads, for instance by taking one of the leads superconducting [11, 12, 13, 14, 15, 16, 17, 18, 19, 20, 21, 22], or by using leads with an inperfect [23] or time-dependent [24] voltage bias. Positive cross-correlations are also expected at finite frequencies, due to the plasmonic screening currents existing in capacitive circuits [10, 25]. It follows from Buttiker's work that obtain-

ing positive cross-correlations at zero frequency without modifying the assumptions on the leads requires to have interactions inside the device. Saito et al. have considered a two dimensional electron gas in the fractional quantum Hall regime, described by a chiral Luttinger liquid theory [26]. Zero-frequency positive cross-correlations can be obtained in this system in the limit of small filling factors, where the excitations of the chiral Luttinger liquid take a bosonic character. This leaves open the question whether interactions localized inside the beam splitter can lead to zero-frequency positive cross-correlations even for a normal fermionic circuit.

Current correlations in a single quantum dot have been studied in the sequential tunneling limit [27, 28, 29, 30], in the cotunneling regime [31, 32] and in the Kondo regime [33]. In the (spin-degenerate) sequential tunneling limit, a sub-Poissonian Fano factor has been found for some two-terminal cases [27, 28, 29], and, for the three-terminal case, cross-correlations are expected to be always negative when the intrinsic level spacing  $E$  of the dot is much smaller than temperature [28]. However, a super-Poissonian Fano factor has been predicted for a two-terminal quantum dot with  $E \ll k_B T$  connected to ferromagnetic leads [30]. In the cotunneling regime, a super-Poissonian Fano factor can be obtained in the two-terminal case [31]. The extent to which this would lead to positive cross-correlations for a three-terminal quantum dot was not clear.

In this article, we consider a three-terminal quantum dot with  $E \ll k_B T$ , operated as a beam splitter: one contact acts as source and the other two as drains. In earlier papers, we have proposed two different ways to obtain zero-frequency positive cross-correlations in this circuit, in the sequential tunneling limit. We have assumed that only one orbital of the dot, i.e. one single-particle level, transports current. Both methods rely on lifting spin-

degeneracy, either by using ferromagnetic leads [34], or by using paramagnetic leads but placing the dot in a magnetic field [35]. Note that in these works, the leads are biased with constant voltages and modeled as non-interacting Fermi gases. Then, with respect to Buttiker's proof, only the hypothesis of the absence of interactions inside the device itself is relaxed. Moreover, in contrast to the system studied in [26], excitations inside the device remain purely fermionic.

We provide here a detailed analysis of the physical origin of the positive cross-correlations found in a three-terminal interacting quantum dot. The essential ingredient is the existence of Coulomb interactions on the dot. (Note that in a spin valve connected to ferromagnetic leads, in which there are no charging effects, the cross-correlations were found to be negative [36]). Here, we assume that Coulomb interactions prevent a double occupancy of the dot. In the limit where only one orbital level of the dot transports current, the mechanism responsible for positive cross-correlations is dynamical spin-blockade. Simply speaking, up- and down-spins tunnel through the dot with different rates. The spins which tunnel with a lower rate modulate the transport through the opposite spin-channel, which leads to a bunching of tunneling events. We consider both the Fano factor in the input lead, called input Fano factor, and the cross-correlations between the two output leads, called output cross-correlations. We show that a super-Poissonian input Fano factor is not equivalent to positive output cross-correlations and identify the conditions to obtain these effects. We furthermore show that there is a direct mapping between the above case of a non spin-degenerate quantum dot with a single orbital-level transporting current and the case of a spin-degenerate quantum dot with two orbital levels transporting current. This mapping implies that the result of [28] cannot be generalized to  $E \ll k_B T$ : cross-correlations are not always negative for a spin-degenerate three-terminal quantum dot. More generally, this result provides the evidence that lifting spin-degeneracy is not necessary for obtaining zero-frequency positive cross-correlations due to interactions inside a beam splitter device, even for a normal fermionic circuit with a perfect voltage bias. In this spin-degenerate case, positive cross-correlations stem from the partial blockade of an electronic channel by another one, thus we propose to call this effect: dynamical channel-blockade.

The present article is organized as follows. Section II develops the mathematical description valid for the one-orbital problem. This one-orbital problem is analyzed for two different configurations. First, the case of ferromagnetic leads and zero magnetic field is treated in Section III. Secondly, the case of a Zeeman splitting created by a magnetic field is treated in Section IV. In Section V, we show how to map the two-orbital spin-degenerate problem onto the one-orbital problem.

## II. MODEL AND GENERAL DESCRIPTION FOR THE ONE-ORBITAL CASE

### A. Model

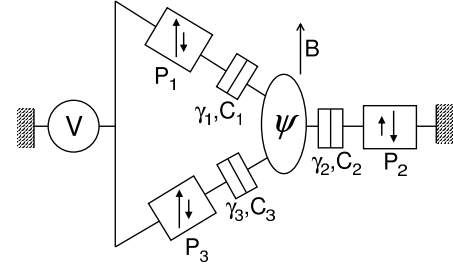


FIG. 1: Electrical diagram of a quantum dot connected to three leads  $i=1,2,3$  with collinear magnetic polarizations  $P_i$ , through tunnel junctions with net tunneling rates  $\gamma_i$  and capacitances  $C_i$ . A bias voltage  $V$  is applied to leads 1 and 3; lead 2 is connected to ground. A magnetic field  $B$  collinear to the lead polarizations is applied to the dot.

We consider a quantum dot connected to three leads  $i=1,2,3$ , through tunnel junctions with capacitances  $C_i$  and net spin-independent tunneling rates  $\gamma_i$  (Fig. 1). The leads are magnetically polarized in collinear directions. We also assume that the dot is subject to a magnetic field  $B$  collinear to the lead polarizations. A voltage bias  $V$  is applied to leads 1 and 3 whereas lead 2 is connected to ground. The voltage  $V$  is considered as positive, such that it is energetically more favorable for electrons to go from the input electrode 2 to the output electrodes 1 or 3 than in the opposite direction. In this section, we also assume that

$$k_B T \ll \mu_B B \ll eV \ll E_C \ll E_0, \quad (1)$$

where the charging energy  $E_C = e^2/2C$  of the dot depends on  $C = \sum_i C_i$ . According to (1), only one orbital level of the dot, with energy  $E_0$ , needs to be taken into account to describe the current transport, and this level cannot be doubly occupied. In this situation, there are three possible states for the dot: either empty i.e.  $n = 0$ , or occupied with one electron with spin  $\uparrow$  or  $\downarrow$  i.e.  $n = 1$ . The magnetic field  $B$  induces a Zeeman splitting of the level according to  $E_{\uparrow(\downarrow)} = E_0 + (\mp) g \mu_B B = 2$ , where  $\mu_B = e\hbar/2m$  is the Bohr magneton. In this article, we will assume  $B \ll 0$ , i.e. the up-spin level is energetically lower than the down-spin level in the presence of a magnetic field. The collinear magnetic polarizations  $P_j$  of the leads are taken into account by using spin-dependent tunneling rates  $\gamma_j^{\uparrow} = \gamma_j(1 + P_j)$  and  $\gamma_j^{\downarrow} = \gamma_j(1 - P_j)$ . In a simple model, the spin-dependence is a consequence of the different densities of states for electrons with up and down spins in the leads [37]. The rate for an electron to

tunnel on/o the dot ( $= + = -1$ ) through junction  $j$  is then given by

$$\Gamma_{j\pm} = \Gamma_j (1 + \exp[(E_{\pm} - eV_j)/k_B T]), \quad (2)$$

where  $V_1 = V_3 = C_2 V = C$  and  $V_2 = (C_1 + C_3)V = C$ . Here, we took the Fermi energy  $E_F = 0$  for lead 2 as a reference. On the dot, there can be spin- $\uparrow$  scattering, due for instance to spin-orbit coupling or to magnetic impurities. According to the detailed balance rule, we write the spin- $\uparrow$  rates as

$$\Gamma_{\# \rightarrow \uparrow} = \Gamma_{\uparrow \rightarrow \#} \exp\left(\frac{g_{\uparrow \downarrow} B}{2k_B T}\right)$$

for the  $\# \rightarrow \uparrow$  transition and

$$\Gamma_{\uparrow \rightarrow \#} = \Gamma_{\# \rightarrow \uparrow} \exp\left(\frac{g_{\uparrow \downarrow} B}{2k_B T}\right)$$

for the  $\uparrow \rightarrow \#$  transition.

#### B. Master equation treatment

In the sequential-tunneling limit  $\Gamma_j \ll k_B T$ , electronic transport through the dot can be described by the master equation [27]

$$\frac{d}{dt} \begin{pmatrix} p_{\uparrow\uparrow}(t) \\ p_{\uparrow\#}(t) \\ p_{\#}(t) \\ p_{\downarrow\#}(t) \\ p_{\downarrow\downarrow}(t) \end{pmatrix} = \mathcal{M} \begin{pmatrix} p_{\uparrow\uparrow}(t) \\ p_{\uparrow\#}(t) \\ p_{\#}(t) \\ p_{\downarrow\#}(t) \\ p_{\downarrow\downarrow}(t) \end{pmatrix}; \quad (3)$$

where  $p_{\alpha\beta}(t)$ ,  $\alpha, \beta \in \{\uparrow, \downarrow, \#\}$ , is the instantaneous occupation probability of state  $\alpha\beta$  at time  $t$ , and where

$$\mathcal{M} = \begin{pmatrix} -\Gamma_{\uparrow\downarrow} & \Gamma_{\downarrow\uparrow} & 0 & 0 & 0 \\ \Gamma_{\uparrow\downarrow} & -\Gamma_{\uparrow\#} & \Gamma_{\# \rightarrow \uparrow} & 0 & 0 \\ 0 & \Gamma_{\uparrow\#} & -\Gamma_{\# \rightarrow \uparrow} - \Gamma_{\# \rightarrow \downarrow} & \Gamma_{\downarrow\#} & 0 \\ 0 & 0 & \Gamma_{\# \rightarrow \downarrow} & -\Gamma_{\downarrow\#} & \Gamma_{\downarrow\uparrow} \\ 0 & 0 & 0 & \Gamma_{\downarrow\uparrow} & -\Gamma_{\downarrow\downarrow} \end{pmatrix} \quad (4)$$

depends on the total rates  $\Gamma_{\alpha\beta} = \Gamma_{\beta\alpha}$ . This master equation treatment relies on a Markovian approximation valid for frequencies  $\omega$  lower than  $\max[k_B T, \min_j (E_{\pm} - eV_j)] \sim [38]$ . From Eq. (3), the stationary occupation probabilities  $p$  are

$$p = \frac{\begin{pmatrix} \Gamma_{\downarrow\uparrow} & \Gamma_{\uparrow\downarrow} & 0 & 0 & 0 \\ 0 & \Gamma_{\uparrow\#} & \Gamma_{\# \rightarrow \uparrow} & 0 & 0 \\ 0 & 0 & \Gamma_{\# \rightarrow \uparrow} + \Gamma_{\# \rightarrow \downarrow} & \Gamma_{\downarrow\#} & 0 \\ 0 & 0 & \Gamma_{\# \rightarrow \downarrow} & \Gamma_{\downarrow\#} & \Gamma_{\downarrow\uparrow} \\ 0 & 0 & 0 & \Gamma_{\downarrow\uparrow} & \Gamma_{\downarrow\downarrow} \end{pmatrix}^{-1} \begin{pmatrix} 0 \\ 0 \\ 0 \\ 0 \\ 0 \end{pmatrix}}{\begin{pmatrix} \Gamma_{\downarrow\uparrow} & \Gamma_{\uparrow\downarrow} & 0 & 0 & 0 \\ 0 & \Gamma_{\uparrow\#} & \Gamma_{\# \rightarrow \uparrow} & 0 & 0 \\ 0 & 0 & \Gamma_{\# \rightarrow \uparrow} + \Gamma_{\# \rightarrow \downarrow} & \Gamma_{\downarrow\#} & 0 \\ 0 & 0 & \Gamma_{\# \rightarrow \downarrow} & \Gamma_{\downarrow\#} & \Gamma_{\downarrow\uparrow} \\ 0 & 0 & 0 & \Gamma_{\downarrow\uparrow} & \Gamma_{\downarrow\downarrow} \end{pmatrix}^{-1} \begin{pmatrix} 0 \\ 0 \\ 0 \\ 0 \\ 0 \end{pmatrix}}, \quad (5)$$

with  $\Gamma_{\alpha\beta} = \Gamma_{\beta\alpha}$ , for  $\alpha, \beta \in \{\uparrow, \downarrow, \#\}$ , and

$$p_0 = 1 - p_{\uparrow\uparrow} - p_{\uparrow\#} - p_{\downarrow\#} - p_{\downarrow\downarrow}. \quad (6)$$

These probabilities can be used to calculate the average value  $\langle I_{ji} \rangle$  of the tunneling current  $I_j(t)$  through junction  $j$  as  $\langle I_{ji} \rangle = \langle I_{j\uparrow} \rangle - \langle I_{j\downarrow} \rangle$ , where  $\langle I_{j\uparrow} \rangle = \langle I_{j\downarrow} \rangle$  is the average current of electrons with spins  $\uparrow$ , and

$$\langle I_{j\uparrow} \rangle = e \sum_{\alpha\beta} p_{\alpha\beta} A_{\alpha\beta}(\uparrow). \quad (7)$$

Here,  $A_{\alpha\beta}(\uparrow)$  is the state of the dot after the tunneling of an electron with spin  $\uparrow$  in the direction  $j$ , i.e.  $A_{\alpha\beta}(\uparrow) = 0$  and  $A_{\alpha\beta}(\uparrow) = 1$ .

The frequency spectrum of the noise correlations can be defined as

$$S_{ij}(\omega) = \frac{1}{2\pi} \int_{-\infty}^{\infty} dt C_{ij}(t) \exp(i\omega t), \quad (8)$$

where

$$C_{ij}(t) = \langle I_i(t) I_j(0) \rangle - \langle I_i(0) \rangle \langle I_j(t) \rangle. \quad (9)$$

Following the method developed in Refs. [27], we can write this spectrum as:

$$S_{ij}(\omega) = S_{ij}^{S^{ch}} + S_{ij}^C(\omega) \quad (10)$$

with  $S_j^{S^{ch}} = \frac{1}{2} S_j^{S^{ch}}$  and  $S_{ij}^C(\omega) = \frac{1}{2} S_{ij}^C(\omega)$ . Here,

$$S_j^{S^{ch}} = 2e^2 \sum_i \langle I_{ji} \rangle^2, \quad (11)$$

is the Schottky noise associated to the tunneling of electrons with spin  $\uparrow$  through junction  $j$ , and, from (3),

$$\frac{S_{ij}^C(\omega)}{2e^2} = \sum_{\alpha\beta} \langle I_{\alpha\beta}(\omega) \rangle \langle I_{\alpha\beta}(\omega) \rangle + \sum_{\alpha\beta} \langle I_{\alpha\beta}(\omega) \rangle \langle I_{\alpha\beta}(\omega) \rangle, \quad (12)$$

with

$$\langle I_{\alpha\beta}(\omega) \rangle = \text{Re} [i\omega \mathcal{M}^{-1} \begin{pmatrix} 0 \\ 0 \\ 0 \\ 0 \\ 0 \end{pmatrix}]_{\alpha\beta}, \quad (13)$$

and  $\mathcal{P}$  the identity matrix. We also define, for later use, the spin components of  $S_{ij}(\omega)$ :

$$S_{ij}(\omega) = S_{ij}^{S^{ch}} + S_{ij}^C(\omega). \quad (14)$$

Due to the existence of the stationary solution  $\mathcal{M} p_0 = 0$ , the matrix  $\mathcal{M}$  has only two non-zero eigenvalues  $\pm i\omega$ , i.e.  $\mathcal{M} v = \pm i\omega v$ , given by

$$v = \frac{1}{2} \begin{pmatrix} \Gamma_{\downarrow\uparrow} \\ \Gamma_{\uparrow\downarrow} \\ \Gamma_{\uparrow\#} \\ \Gamma_{\downarrow\#} \\ \Gamma_{\downarrow\downarrow} \end{pmatrix} < 0,$$

with

$$v = \begin{pmatrix} \Gamma_{\downarrow\uparrow} \\ \Gamma_{\uparrow\downarrow} \\ \Gamma_{\uparrow\#} \\ \Gamma_{\downarrow\#} \\ \Gamma_{\downarrow\downarrow} \end{pmatrix}$$

and

$$v = \begin{pmatrix} \Gamma_{\downarrow\uparrow} \\ \Gamma_{\uparrow\downarrow} \\ \Gamma_{\uparrow\#} \\ \Gamma_{\downarrow\#} \\ \Gamma_{\downarrow\downarrow} \end{pmatrix} + \begin{pmatrix} \Gamma_{\downarrow\uparrow} \\ \Gamma_{\uparrow\downarrow} \\ \Gamma_{\uparrow\#} \\ \Gamma_{\downarrow\#} \\ \Gamma_{\downarrow\downarrow} \end{pmatrix}.$$

Then, the matrix  $\mathcal{M}$  can be written in the form  $\mathcal{M} = \mathcal{R}^{-1} + \mathcal{P}_+ + \mathcal{P} \mathcal{R}$ , where  $\mathcal{R}$  is a reversible  $3 \times 3$  matrix, and  $\mathcal{P}_+(\cdot)$  is a  $3 \times 3$  matrix with the element 1 at the first (second) row and first (second) column. Accordingly,  $\mathcal{G}(\omega)$  can be written as

$$\mathcal{G}(\omega) = \frac{\mathcal{A}^+}{\omega^2 + \frac{\gamma}{2}} + \frac{\mathcal{A}}{\omega^2 + \frac{\gamma}{2}}, \quad (15)$$

with  $\mathcal{A} = \mathcal{R}^{-1} \mathcal{P} \mathcal{R}$ . Therefore, we have

$$S_{ij}^c(\omega) = \sum_{s=1}^X \frac{S_{ij}^s}{\omega^2 + \frac{\gamma_s}{2}}, \quad (16)$$

where  $S_{ij}^s$  follows from Eqs. (12) and (15). The total Schottky noise  $S_j^{sch}$  through junction  $j$  is a white noise due to the hypothesis of instantaneous tunneling. For a single junction biased by a voltage source, one would get only this term. However, in the spectrum  $S_{ij}(\omega)$ , interactions don't come into play only through the frequency dependent term (16). Interactions also modify the values of the terms  $h_{ji}$  determining the Schottky noise. Note that at high frequencies  $\omega \gg \gamma_j$ , we have  $S_{ij}(\omega) = S_j^{sch}$ . If we furthermore assume  $V = V_{max}^{sgn(E_0)}$ ,  $S_j^{sch} = 2e \hbar I_{ji}$  thus  $S_{ij}(\omega)$  becomes Poissonian, i.e.  $S_{ij}(\omega) = 2e \hbar I_{ji}$ .

In the three-terminal case studied here, we will be interested in the input Fano factor

$$F_2 = \frac{S_{22}(\omega = 0)}{2e \hbar I_2},$$

and in the output cross-Fano factor

$$F_{13} = \frac{S_{13}(\omega = 0)}{2e \hbar I_1}.$$

We also define the resonance voltages

$$V_0 = E_0 j \frac{C}{eC_2}$$

and

$$V_0^+ = E_0 j \frac{C}{e(C_1 + C_3)}.$$

Since we consider  $V > 0$  only, at  $B = 0$ , for  $E_0$  positive (negative), the dot orbital arrives at resonance with the Fermi level of the input (the outputs) when  $V = V_0^{+(\cdot)}$ . If a magnetic field is applied, each of these voltage resonances is split into two resonances

$$V_{n(\#)} = V_0 + \left( \pm \right) \frac{g_B B C}{2eC_2}$$

and

$$V_{n(\#)}^+ = V_0^+ + \left( \pm \right) \frac{g_B B C}{2e(C_1 + C_3)},$$

associated to the  $n(\#)$  levels respectively because we consider  $B > 0$  only. We expect  $F_2$  and  $F_{13}$  to show strong variations for  $V \approx V_{n(\#)}^{sgn(E_0)}$ .

### C. Time-domain analysis

The correlation function  $C_{ij}(t)$  can be obtained from the inverse Fourier transform of Eqs. (10), (11) and (16):

$$C_{ij}(t) = \langle i | S_j^{sch}(t) | j \rangle + \sum_{s=1}^X \frac{S_{ij}^s}{2\gamma_s} \exp(-\gamma_s t). \quad (17)$$

In the sequential tunneling limit, tunneling events occur one by one, thus

$$\lim_{t \rightarrow 0^+} C_{ij}(t) = 2\hbar I_{ji} < 0. \quad (18)$$

Let us first focus on the spin-degenerate case, that is  $\gamma_n = \gamma_{\#}$  for  $j = 1, 2, 3$ . In this case, the eigenvectors  $v_{\pm}$  of  $\mathcal{M}$  correspond to the spin/charge excitations of the system (i.e.  $v_+ = [1; 1; 0]$ ,  $v_- = [1; -1; 2]$ ), and  $\gamma_{\pm}$  to their relaxation rates. This is directly connected to the fact that in the spin-degenerate case,  $S_{ij}^+ = 0$ , thus  $S_{ij}(\omega) = S_j^{sch}$  is a Lorentzian function and  $C_{ij}(t) = \langle i | S_j^{sch}(t) | j \rangle = S_j^{sch} \exp(-\gamma_j t)$ . This last equation implies that, for any time,  $C_{22}(t) = S_2^{sch}$  and  $C_{13}(t)$  keep the same sign, which is negative according to Eq. (18). Thus, in the spin-degenerate one-orbital case,  $F_2$  is always sub-Poissonian and  $F_{13}$  always negative. When spin-degeneracy is lifted,  $v_{\pm}$  both become a linear combination of the charge and spin excitations. Thus, having  $S_{ij}^+ \neq 0$  is not forbidden anymore. Eqs. (17), and (18) altogether with  $\gamma_+ < \gamma_-$  imply that if  $S_{ij}(\omega = 0) > S_j^{sch}$ , one has  $S_{ij} < 0$  and  $S_{ij}^+ > 0$ . Therefore, in the one-orbital case, a positive sign for  $F_2 = S_2^{sch}/2e\hbar I_2$  and  $F_{13}$  can only be due to terms in  $\gamma_+$ .

The results obtained for  $C_{ij}(t)$  can be put in perspective with some fundamental quantities like the average dwell time  $\tau$  of spins on the dot and the average delay  $t_0$  between the occupancy of the dot by two consecutive electrons. These quantities can be calculated for  $\gamma_{sf} = 0$  as

$$\tau = \sum_j \frac{4e^2 p}{S_j^{sch}} \quad (19)$$

and

$$t_0 = \sum_j \frac{4e^2 p_0}{S_j^{sch}}. \quad (20)$$

The noise reaches its high-voltage limit once  $V_{\text{max}}^{\text{sgn}(E_0)} = \max(V^{\text{sgn}(E_0)})$  with  $V_{\text{max}}^+ = V_{\#}^+$  and  $V_{\text{max}}^- = V_{\#}^-$ . In this limit, the current transport is unidirectional, i.e.  $I_{2;+} = 0$  and  $I_{j;+} = 0$  and for any  $j \neq 2$  and  $j \neq \#$ . Thus, Eqs. (19) and (20) lead to  $t_0 = 1/2$  and  $t = 1/(1 + 3)$ . The average number

$$n_b = \frac{S_{2\#}^{\text{sch}}}{S_{2\#}^{\text{sch}}} \quad (21)$$

of up spins crossing the input junction between two consecutive down spins for  $s_f = 0$ , which becomes  $n_b = I_{2\#} = I_{2\#}$  for  $V = V_{\text{max}}^{\text{sgn}(E_0)}$ , is also of importance. It can be used to calculate the average duration

$$t_b = n_b t_0 + (n_b + 1) t_0 \quad (22)$$

between the occupation of the dot by two consecutive down spins for  $s_f = 0$ . In Section III C, the analysis of  $C_{ij}(t)$  will be supplemented by simulating numerically the time evolution of the spin of the dot. As expected, these simulations are in agreement with the results obtained from the master equation approach, but their interest is to allow a visualization of  $\dot{\sigma}(t)$ .

#### D. Relation between $F_2$ and $F_{13}$

The average input current  $\langle I_{2i} \rangle$  and the input Fano factor  $F_2$  in a three-terminal device correspond to the average current and the Fano factor in a two-terminal device where the output leads 1 and 3 are replaced by an effective output with a net spin-independent tunneling rate  $t = t_1 + t_3$  and with an effective polarization  $P_{\text{out}} = (P_1 + P_3)/2$ . Then, one fundamental question to answer is whether there is a simple relation between  $F_2$  and  $F_{13}$  in the three-terminal circuit. Charge conservation and the finite dispersion of  $j_{\text{dot}}(t)$  lead to [27]

$$S_{22}(! = 0) = S_{11}(! = 0) + S_{33}(! = 0) + 2S_{13}(! = 0). \quad (23)$$

At high voltages  $V = V_{\text{max}}^{\text{sgn}(E_0)}$ , the unidirectionality of current transport and the average-currents conservation lead to  $S_2^{\text{sch}} = S_1^{\text{sch}} + S_3^{\text{sch}}$ . In this limit, Eqs. (10) and (23) imply that

$$S_{22}^c(! = 0) = S_{11}^c(! = 0) + S_{33}^c(! = 0) + 2S_{13}^c(! = 0). \quad (24)$$

Since the voltage bias is the same for leads 1 and 3, we have  $g_1 = g_3$  for  $\beta = 1$ . Then, from (12), in our singly-occupied one-orbital case, Eq. (24) leads to

$$S_{22}^c(! = 0) = \sum_{i,j} \frac{(t_1 + t_3)(t_{10} + t_{30})}{t_1 t_3} S_{1i;3j}^c(! = 0).$$

If we furthermore assume  $P_1 = P_3$ , the ratio  $F_1 = F_3 = 1/3$  is independent of  $t$  and

$$F_{13} = (F_2 - 1) \frac{1 - 3}{2}. \quad (25)$$

In summary, for the one-orbital circuit studied here, there exists a simple relation between  $F_2$  and  $F_{13}$  when  $P_1 = P_3$  and  $V = V_{\text{max}}^{\text{sgn}(E_0)}$ . Note that the derivation of property (25) requires neither  $s_f = 0$ , nor  $B = 0$ . On the contrary, the voltage-bias configuration used is crucial. Indeed, if the three leads 1, 2, 3, were for instance biased at voltages  $V, V/2$  and 0 respectively, the current transport would not be unidirectional even in the high  $V$  limit. When property (25) is verified, a super-Poissonian (sub-Poissonian)  $F_2$  is automatically associated with positive (negative) zero-frequency cross-correlations. However, Sections III and IV, which also treat this one-orbital case, illustrate that when  $P_1 \neq P_3$  or  $V \neq V_{\text{max}}^{\text{sgn}(E_0)}$ , property (25) is not valid anymore, and in particular a super-Poissonian  $F_2$  can be obtained without a positive  $F_{13}$ . In Section IV B,  $F_2$  and  $F_{13}$  even show variations which are qualitatively different:  $F_{13}$  displays a voltage resonance not present in  $F_2$ . Thus, even for the one-orbital quantum dot circuit studied here, the three-terminal problem is in general not trivially connected to the two-terminal problem.

The main ingredients for deriving (25) are the unidirectionality of current transport and a division of current between the two outputs identical for the two spin directions. One can wonder whether any tunnel-junction circuit with a geometry analogous to that of Figure 1 satisfies property (25) for  $V = V_{\text{max}}^{\text{sgn}(E_0)}$  and  $P_1 = P_3$ . Indeed, it is sometimes the case. For instance, Borlin et al. have studied at  $T = 0$  a normal metal island too large to have charging effects, connected, through tunnel junctions, to one superconducting or normal input lead and to two normal output leads with  $P_1 = P_3 = 0$  placed at the same output potential [17]. For this system, in both the hybrid and the normal cases, a relation analog to (25) is fulfilled, provided  $F_1 = F_3$  is replaced by  $g_1 = g_3$ , where  $g_1$  and  $g_3$  are the conductances of the output junctions. In spite of this, (25) is not universal even for spin-degenerate tunnel-junction circuits. This can be shown by considering the circuit of Fig. 1, with  $B = 0, P_1 = P_2 = P_3 = 0$  and a two-orbital dot (Section V). In this case, the division of currents between the two outputs will generally depend on the orbital considered, because of the different spatial extensions of the orbitals and of the asymmetric positions of the output leads with respect to them [39]. One has to assume that the division of currents between leads 1 and 3 is independent of the orbital considered in order to recover property (25) at  $V = V_{\text{max}}^{\text{sgn}(E_0)}$ .

### E. Influence of screening currents at non-zero frequencies

The total instantaneous current  $I_j^{\text{tot}}(t)$  passing through branch  $j$  includes the tunneling current  $I_j(t)$  but also the screening currents needed to guarantee the electrostatic equilibrium of the capacitors after a tunneling event through any junction  $i \in \{1, 2, 3\}$ . However, screening currents contribute neither to the average value  $\langle I_j^{\text{tot}} \rangle$  of the total current  $I_j^{\text{tot}}(t)$ , i.e.  $\langle I_j^{\text{tot}} \rangle = \langle I_j \rangle$ , nor to the low frequency part of the total current correlations  $S_{ij}^{\text{tot}}(\omega)$ , i.e.  $S_{ij}^{\text{tot}}(\omega) = S_{ij}(\omega) = 0$  for  $\omega \rightarrow 0$  because, in average, the screening currents due to tunneling through the different junctions compensate each other at zero frequency (see for instance [1]). Screening currents contribute to  $S_{ij}^{\text{tot}}(\omega)$  only once  $S_{ij}(\omega)$  deviates from its zero-frequency limit. In the following, we will assume that the cutoff frequency  $\omega_c$  is much larger than the inverse of the collective response times associated to the charging of the capacitors. This is equivalent to assuming that, on the time scale on which  $\dot{n}_{\text{dot}}(t)$  varies, any charge variation of the dot triggers instantaneously the screening currents needed for its compensation:

$$I_j^{\text{tot}}(t) = I_j(t) + \sum_i \frac{C_j}{C_i} I_i(t). \quad (26)$$

According to this approximation, the total current correlations  $S_{ij}^{\text{tot}}(\omega)$ , including screening currents, can be written as

$$S_{ij}^{\text{tot}}(\omega) = \sum_{n,m} \left( \delta_{in} \frac{C_i}{C} + \delta_{jm} \frac{C_j}{C} \right) S_{nm}(\omega). \quad (27)$$

The sign of these total current cross-correlations is not trivial. This problem is addressed in Section III E.

### III. ONE-ORBITAL QUANTUM DOT CONNECTED TO FERROMAGNETIC LEADS, IN THE ABSENCE OF A MAGNETIC FIELD

Here, we focus on the one-orbital case introduced in Section II, for  $B = 0$  and magnetically polarized leads. In the absence of a magnetic field, one single resonance is expected in the voltage characteristics, for  $V > V_0^{\text{sgn}(E_0)}$ . Figures 2 to 7 show curves for a constant value of the polarization amplitudes  $P_1 = P_2 = P_3 = 0.6$ . This corresponds for instance to having the different leads made out of the same ferromagnetic material.

#### A. Zero-frequency results for $E_0 > 0$

We first consider the case in which the orbital level  $E_0$  is above the Fermi level of the leads at equilibrium ( $E_0 > 0$ ). The typical voltage dependence of the average

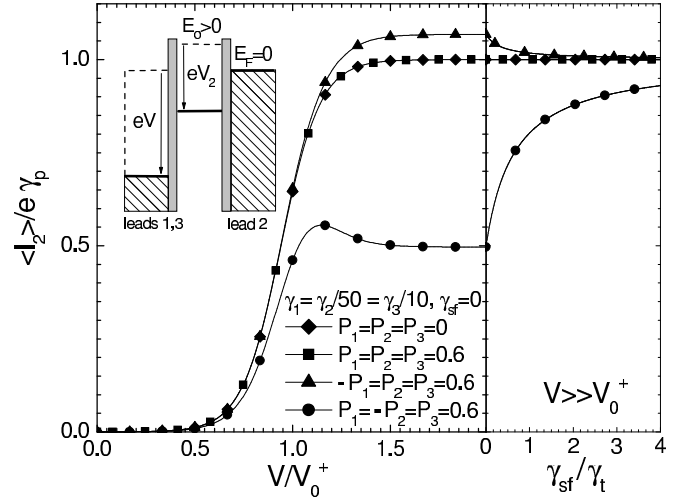


FIG. 2: Left panel: Current-voltage characteristic of the circuit of Fig. 1, for  $E_0 > 0$ ,  $C_1 = C_2 = C_3$ ,  $\gamma_1 = \gamma_2 = 50 = \gamma_3 = 10$ ,  $k_B T = \hbar \omega_0 / 2 = 0.1$ ,  $B = 0$ , and different values of lead polarizations. The average current  $\langle I_2 \rangle$  through lead 2 is plotted in units of its paramagnetic high voltage limit  $e_p = 2e\gamma_2(1 + \gamma_3) = (1 + 2\gamma_2 + \gamma_3)$ ; the voltage in units of the resonance voltage  $V_0^+$  (see II B). For  $P_1 = P_2 = P_3$  (squares),  $\langle I_2 \rangle$  coincides with the paramagnetic case (diamonds). In the other cases, the high-voltage limit of  $\langle I_2 \rangle$  can be larger or smaller than the paramagnetic value, depending on the lead polarizations. The inset shows the electrochemical potentials in the circuit. Notation  $E_F$  refers to the Fermi level in lead 2. (In all the plots, potentials are shown for the case where the dot is empty). Right panel: Influence of spin-1/2 scattering in the high-voltage limit  $V \gg V_0^+$ . Here, the spin-1/2 scattering rate  $\gamma_{sf}$  is expressed in units of  $\tau = 1 + \gamma_3$ . Spin-1/2 scattering makes the  $\langle I_2 \rangle(V)$  curve tend to the paramagnetic one.

input current  $\langle I_2 \rangle$  is shown in the left panel of Fig. 2. This current is exponentially suppressed at low voltages, increases around the voltage  $V_0^+$  and saturates at higher voltages. The width on which  $\langle I_2 \rangle$  varies is of the order of  $V \sim 10k_B T C = e(C_1 + C_3)$ . The high-voltage limit of  $\langle I_2 \rangle$  depends on the polarizations  $P_i$  and rates  $\gamma_i$  but not on the capacitances  $C_i$  because the tunneling rates saturate at high voltages [see Eq. (2)]. For the paramagnetic case, this limit is

$$e_p = e \frac{2\gamma_2\tau}{\tau + 2\gamma_2}. \quad (28)$$

In this last expression,  $\gamma_2$  is weighted by a factor 2 to account for both the populations of up and down spins arriving from the input lead. The rate  $\tau = 1 + \gamma_3$  is not weighted by such a factor because there can be only one electron at a time on the dot, which can tunnel to the output leads with the total rate  $\tau$ . For a sample with magnetic contacts, the high-voltage limit of  $\langle I_2 \rangle$  can be higher or lower than  $e_p$ , depending on the parameters considered. Indeed, for  $V \gg V_0^+$ , we have  $I_2(P_1; P_2; P_3) \xrightarrow{V \gg V_0^+} I_2(0; 0; 0) = e_{p, \text{pouth dot}}$ , where

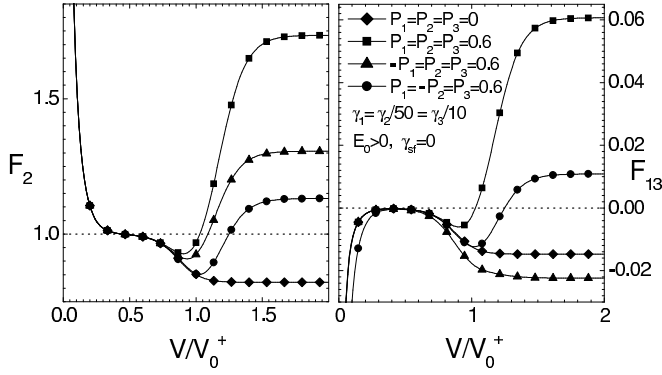


FIG. 3: Input Fano factor  $F_2 = S_{22} (! = 0) = 2eI_2$  (left panel) and output cross-Fano factor  $F_{13} = S_{13} (! = 0) = 2eI_{13}$  between leads 1 and 3 (right panel) as a function of the bias voltage  $V$  for  $\gamma_{sf} = 0$ . The curves are shown for the same circuit parameters as in Fig. 2. When  $P_1 = P_2 = P_3$  (squares),  $F_2$  is different from that of the paramagnetic case (diamonds) in contrast to what happens for  $hI_2$ . At high enough voltages, the cross-correlations are positive in the cases  $P_1 = P_2 = P_3 = 0.6$  (circles) and  $P_1 = P_2 = P_3 = -0.6$ . Note that the sign of the cross-correlations can be reversed by changing the sign of  $P_1$ . The case  $P_1 = P_2 = P_3 = 0.6$  (triangles) illustrates that having a super-Poissonian  $F_2$  is not sufficient to obtain a positive  $F_{13}$ .

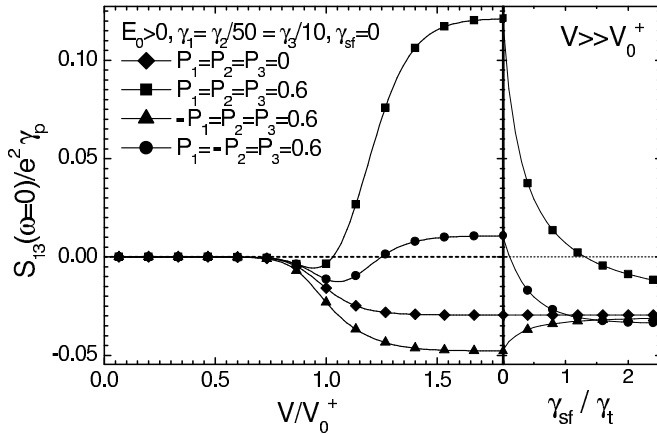


FIG. 4: Zero-frequency cross-correlations  $S_{13} (! = 0)$  between leads 1 and 3 as a function of the bias voltage  $V$  for  $\gamma_{sf} = 0$  (left panel) and as a function of  $\gamma_{sf}$  for  $V \gg V_0^+$  (right panel). The curves are shown for the same circuit parameters as in Fig. 2. In the paramagnetic case (diamonds), spin- $\uparrow$  scattering has no effect. In the limit of large  $\gamma_{sf}$ , cross-correlations tend to the paramagnetic value.

$P_{out} = (P_1 + P_3)/2$  is the net output lead polarization, and where  $h_{dot} = (P_2 - P_{out})$  is the average spin of the dot. Here,  $h_{dot}$  is a positive function of the polarizations, tunneling and scattering rates, which tends to 0 at large  $\gamma_{sf}$ . For  $P_1 = P_2 = P_3$ , the current is the same as in the paramagnetic case because the populations of spin are matched between the input and the output, thus  $h_{dot} = 0$ . Having a saturation current different from

the paramagnetic case requires  $P_{out} \neq 0$  and  $h_{dot} \neq 0$ . When  $P_{out} > P_2$ , the high-voltage limit of  $hI_2$  is lower than that of the paramagnetic case because the spins in minority at the output block the dot, which leads to a  $h_{dot}$  with the same sign as  $P_{out}$ . In this case,  $hI_2$  can show negative differential resistance above  $V_0^+$ , due to the deblockade of the dot by thermal fluctuations which can send back the blocking spins to electrode 2 for  $V > V_0^+$  [30]. Spin- $\uparrow$  scattering modifies the  $hI_2(V)$  curve once  $\gamma_{sf}$  is of the order of the tunneling rates. It suppresses spin accumulation and makes the  $hI_2(V)$  curve tend to the paramagnetic one.

Figure 3 shows  $F_2$  and  $F_{13}$  as a function of  $V$  for  $\gamma_{sf} = 0$ . We also show in Fig. 4 the zero-frequency cross-correlations  $S_{13} (! = 0)$  because it is the signal measured in practice. Well below  $V_0^+$ ,  $S_{13} (! = 0)$  is exponentially suppressed like  $hI_2$  because there are very few tunneling events. In this regime, the dot is empty most of the time, and when an electron arrives on the dot, it leaves it with a much higher rate ( $\gamma_t$ ): the electronic transport is limited only by thermally activated tunneling through junction 2. Tunneling events are thus uncorrelated and  $F_2$  is Poissonian, with a unitary plateau following the thermal divergence  $2k_B T = eV$  occurring at  $V = 0$ . For the same reasons,  $F_{13}$  displays a zero plateau after a polarization-dependent thermal peak at  $V = 0$ . Around  $V \sim V_0^+$ ,  $F_2$ ,  $F_{13}$  and  $S_{13} (! = 0)$  strongly vary. The high-voltage limit depends on tunneling rates and polarizations. In the paramagnetic case, the high-voltage limit of  $F_2$  lies in the interval  $[1; 2]$ , and that of  $F_{13}$  in  $[-1; 0]$ . In the ferromagnetic case, the high-voltage limit of  $F_2$  can be either sub- or super-Poissonian, as already pointed out in the two-terminal case [30]. Spin accumulation is not a necessary condition for having a super-Poissonian  $F_2$ , as can be seen for  $P_1 = P_2 = P_3$ , where  $h_{dot} = 0$ : Negative differential resistance is not necessary either (see case  $P_1 = P_2 = P_3 = 0.6$  in Figs. 2 and 3). Cross-correlations can be either positive or negative depending on the parameters considered, as shown by Figs. 3 and 4. Interestingly, the sign of cross-correlations can be switched by reversing the magnetization of one contact. The case  $P_1 = P_2 = P_3 = 0.6$  of Figs. 3, 4 corresponds to a super-Poissonian  $F_2$  and a positive  $F_{13}$ . The case  $P_1 = P_2 = P_3 = -0.6$  shows that a super-Poissonian  $F_2$  is not automatically associated with positive output cross-correlations. In this case, the cross-correlations are even more negative than in the paramagnetic case. This will be explained physically in Section III C.

The effect of spin- $\uparrow$  scattering on  $S_{13} (! = 0)$  is shown in the right panel of Fig. 4. In the paramagnetic case, spin- $\uparrow$  scattering has no effect on  $S_{13} (! = 0)$ . In the ferromagnetic case, when  $\gamma_{sf}$  is of the order of the tunneling rates,  $S_{13} (! = 0)$  is modified. In the high- $\gamma_{sf}$  limit, cross-correlations tend to the paramagnetic case for any value of the polarizations. Thus, strong spin- $\uparrow$

scattering suppresses positive cross-correlations. However, in practice, it is possible to make quantum dots connected to ferromagnetic leads with spin- $\uparrow$  rates much smaller than the tunneling rates [40]. Hence, spin- $\uparrow$  scattering should not be an obstacle for observing positive cross-correlations in the quantum-dot circuit studied here.

B. Zero-frequency results for  $E_0 < 0$

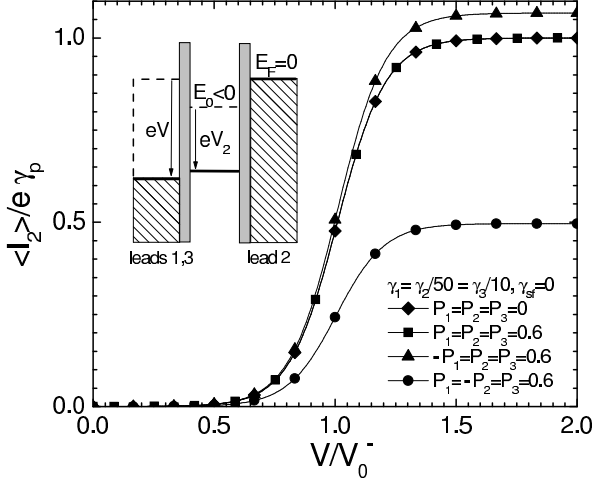


FIG. 5: Current-voltage characteristic of the circuit of Fig. 1 for  $E_0 < 0$ . The polarizations, tunnel rates, capacitances and reduced temperature  $k_B T = E_0$  used are the same as in Fig. 2, plotted for  $E_0 > 0$ . The results differ from the case  $E_0 > 0$  only for  $V < V_0$ .

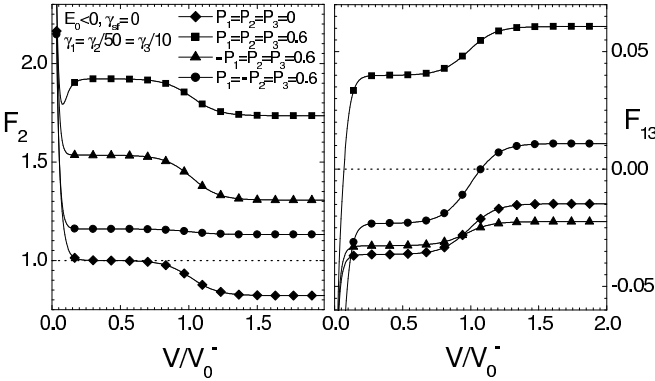


FIG. 6: Input Fano factor  $F_2$  and cross-Fano factor  $F_{13}$  as a function of the bias voltage  $V$ . The curves are shown for the same circuit parameters as in Fig. 5.

We now discuss the case in which the orbital level  $E_0$  is below the Fermi level of the leads at equilibrium ( $E_0 < 0$ ). First, in the low voltage limit in which very few electrons can flow through the device,  $\langle I_2 \rangle$  and  $S_{13} (! = 0)$  exponentially tend to zero like in the case

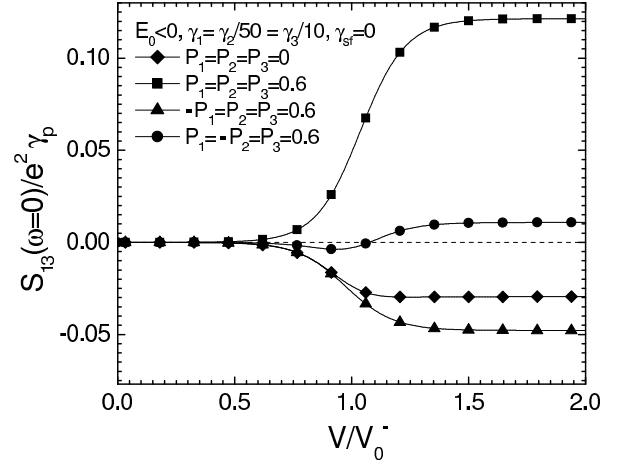


FIG. 7: Zero-frequency current cross-correlations  $S_{13} (! = 0)$  between leads 1 and 3 as a function of the bias voltage  $V$ . The curves are shown for the same circuit parameters as in Fig. 5.

$E_0 > 0$  (Figs. 5 and 7). However, for  $F_2$  and  $F_{13}$ , the results differ (Fig. 6). Above the  $2k_B T = eV$  thermal peak, the low voltage plateau of  $F_2$  is always super-Poissonian for  $P_{out} \neq 0$ . Above a polarization-dependent thermal peak,  $F_{13}$  displays a low voltage plateau which is either negative or positive. These features indicate a correlated transfer of charges in spite of the thermally activated limit. In fact, for  $V < V_0$ , the dot is occupied most of the time and the electronic transport is limited by thermally activated tunneling through the output junctions 1 and 3. In these conditions, contrarily to what happens for  $E_0 > 0$ , the polarization of the output leads comes into play even for  $V \neq 0$ . Indeed, when  $P_{out} \neq 0$ , the spins in minority at the output have less chances to leave the dot under the effect of thermal fluctuations. In the intermediate voltage range  $V < V_0$ , the quantities  $\langle I_2 \rangle$ ,  $F_2$ ,  $F_{13}$  and  $S_{13} (! = 0)$  differ from the case  $E_0 > 0$ . However, at  $V = V_0$ , they take the same values as for  $E_0 > 0$  and  $V = V_0^+$ . In this high-voltage limit, the effect of spin- $\uparrow$  scattering is identical to that of the case  $E_0 > 0$ . In particular, the right panels of Figs. 2 and 4 are also valid for  $E_0 < 0$ .

### C. Interpretation of these zero-frequency results: Dynamical Spin-Blockade

In this Section, we provide a physical explanation for the results of Sections IIIA and IIIB, in the high-voltage limit  $V = V_0^{\text{sgn}(E_0)}$ , where the sign of  $E_0$  does not matter. This analysis relies on the evaluation of quantities defined in Section IIA and IIB (Table I), on numerical simulations of the temporal evolution of the spin dot of the dot (Fig. 8) and on plots of the correlation functions  $C_{13}(t)$  (Fig. 9).



case	$\frac{S_{13}}{e^2 p}$	$\frac{S_{1\uparrow;3\uparrow}}{e^2 p}$	$\frac{S_{1\downarrow;3\downarrow}}{e^2 p}$	$\frac{S_{1\uparrow;3\downarrow}}{e^2 p}$	$\frac{S_{1\downarrow;3\uparrow}}{e^2 p}$	$\frac{I_{1\uparrow}}{I_{3\uparrow}}$	$\frac{I_{1\downarrow}}{I_{3\downarrow}}$	$n_b$
	-0.030	-0.007	-0.007	-0.007	-0.007	0.1	0.1	1
	0.121	0.149	-0.013	-0.007	-0.007	0.1	0.1	4
N	-0.048	0.026	-0.029	-0.003	-0.042	0.025	0.4	4
	0.011	0.005	-0.011	0.008	0.008	0.1	0.1	0.25

case	$p^\uparrow$	$p^\downarrow$	$p_0$	$p^\uparrow t_\uparrow$	$p^\downarrow t_\downarrow$	$p^\uparrow t_0$	$t_b^\uparrow$	$\frac{p^\uparrow}{j^\uparrow - j^\downarrow}$	$\frac{p^\downarrow}{j^\uparrow + j^\downarrow}$
	0.450	0.450	0.100	0.90	0.90	0.10	1.10	0.09	0.90
	0.450	0.450	0.099	0.56	2.25	0.10	2.75	0.09	1.46
N	0.516	0.378	0.106	0.60	1.77	0.10	2.91	0.09	1.31
	0.055	0.895	0.049	0.563	2.25	0.10	0.25	0.09	0.68

TABLE I: Top: Zero-frequency output cross-correlations  $S_{13}$  ( $! = 0$ ) and its spin contributions  $S_{1\uparrow;3\uparrow}$  ( $! = 0$ ), division  $I_{1\uparrow} = I_{3\uparrow}$  of spin currents between leads 1 and 3 and average number  $n_b$  of up spins crossing the input junction between two consecutive down spins, for the high-voltage limit  $V \gg V_0^{\text{sing}(E_0)}$  of the cases studied in Sections IIIA and IIIB (Figs. 2 to 7). Bottom: Probabilities  $p$  and comparison of the different timescales of the system, for the same parameters (The summation rules (6) and (14) are not exactly verified by the values given in this table because of the limitation in the number of digits).

Let us first focus on the case  $P_1 = P_2 = P_3 = 0.6$  (squares in Table I). For these values of lead polarization, up spins are in the majority at the output. Thus, the dwell times of down spins on the dot is longer than that of up spins ( $t_\downarrow > t_\uparrow$  in Table I). However, one has  $p_\uparrow = p_\downarrow$  thus  $\hbar \dot{\sigma}_{\text{dot}} = 0$ . This is because  $t_\downarrow > t_\uparrow$  is perfectly compensated by the fact that, due to  $P_2 > 0$ , up electrons are in the majority in  $I_2(t)$ . Property  $t_\downarrow > t_\uparrow$  suggests that the up spins can flow through the dot only in short time windows where the current transport is not blocked by a down spin. This situation of "dynamical spin-blockade" is responsible for a bunching of the tunneling events associated to the up spins, as confirmed by the numerical simulations of  $\sigma_{\text{dot}}(t)$  (Fig. 8). The average number of up spins grouped in a "bunch" corresponds to the quantity  $n_b$  given in Table I (see [41]). On the one hand, the phenomenon of up-spins bunching is very strong since, here,  $n_b = 4$ . On the other hand, one can see that the positive sign of  $S_{13}$  ( $! = 0$ ) stems from the up-up correlations (see  $S_{1\uparrow;3\uparrow}$  ( $! = 0$ )  $> 0$  in Table I). Therefore, one question to answer is whether the positive sign of  $S_{13}$  ( $! = 0$ ) can be attributed to this bunching of up-spins tunneling events. For that purpose, we have plotted the correlation function  $C_{13}(t)$  (Fig. 9) and compared it to the characteristic time scales of the electronic transport. The correlation function  $C_{13}(t)$  is negative for times shorter than (approximately) the average delay  $t_0$  between the occupancy of the dot by two consecutive electrons. Then,  $C_{13}(t)$  becomes positive and reaches a maximum at a time comparable to the aver-

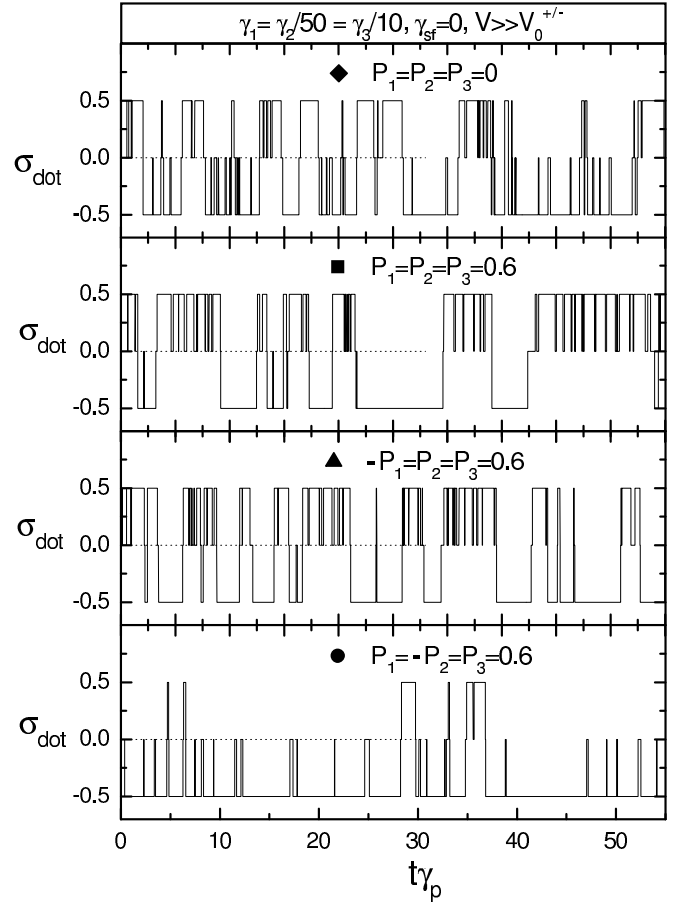


FIG. 8: Numerical simulation of the spin dot of the dot as a function of time in the limit  $V \gg V_0^{\text{sing}(E_0)}$ , for the different cases considered in Figs. 2 to 7.

age delay  $t_0 + t_\uparrow$  between the passage of two up spins on the dot. Eventually,  $C_{13}(t)$  is strongly decreased at times of the order of the average duration  $t_b$  of the "bunch" of spins. Hence, the time-dependence of  $C_{13}(t)$  allows us to attribute the positive value of  $S_{13}$  ( $! = 0$ ) to the bunching of tunneling events caused by dynamical spin-blockade. The same reasoning can be made to explain the super-Poissonian value of  $F_2$  (data not shown).

In the case  $P_1 = P_2 = P_3 = 0.6$  (triangles in Table I), the temporal evolution of  $\sigma_{\text{dot}}$  (see Fig. 8) is qualitatively similar to that of the case  $P_1 = P_2 = P_3 = 0.6$ , thus up-up correlations caused by dynamical spin-blockade lead again to a super-Poissonian  $F_2$ . However, less up electrons flow through lead 1 than in the previous case because the polarization  $P_1$  has been reversed (see  $I_{1\uparrow} = I_{3\uparrow}$  in Table I). Hence, the positive term  $S_{1\uparrow;3\uparrow}$  ( $! = 0$ ) is not large enough to lead to a positive  $S_{13}$  ( $! = 0$ ).

In the case  $P_1 = P_2 = P_3 = 0.6$  (circles in Table I), there is still dynamical spin-blockade, as shown by  $t_\downarrow > t_\uparrow$  in Table I. This dynamical spin-blockade induces again a bunching of the tunneling of up spins (see  $S_{1\uparrow;3\uparrow}$  ( $! = 0$ )  $> 0$  in Table I). However, the up-up correlations are

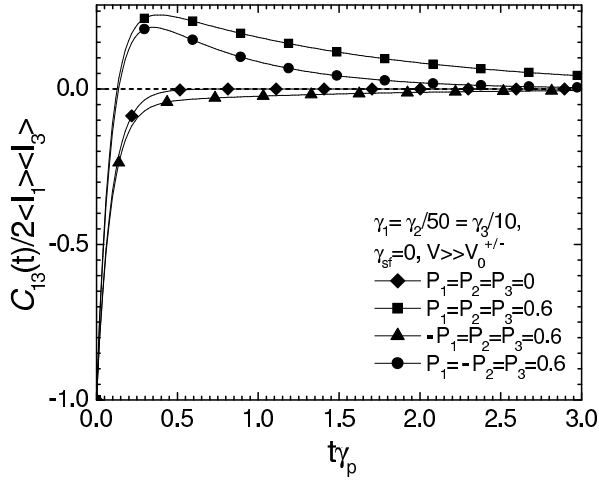


FIG. 9: Time dependence of  $C_{13}(t)$  in the limit  $V = V_0^{\text{sgn}(E_0)}$ , for the different cases considered in Figs. 2 to 7. Note that  $C_{13}(t)$  is given in units of  $G_3(t=0) = 2hI_1hI_3i$ , which depends on the polarization values.

much weaker than in the  $P_1 = P_2 = P_3 = 0.6$  case due to the minority of up spins at the input. Another positive contribution to the cross-correlations stems from the up-down terms (see  $S_{1,3}(\omega=0) > 0$  in Table I). In fact, since the average number  $n_b = 0.25$  of up spins passing consecutively through the dot is very low [41], we have  $t_b < t_\#$ . Then, each up spin is positively correlated to the first down spin preceding him (see Fig. 9). As a result, dynamical spin-blockade now produces a bunching of tunneling events responsible for up-up and up-down correlations. The correlation function  $C_{13}(t)$  differs from that of the case  $P_1 = P_2 = P_3 = 0.6$  in the sense that it decreases more quickly after its maximum, due to the smaller value of  $t_b$ . However, contrarily to the case  $P_1 = P_2 = P_3 = 0.6$ , the decay time of  $C_{13}(t)$  is much larger than  $t_b$ , due to fluctuations in the number of spins per bunch with respect to  $n_b = 0.25$  (Fig. 8).

In conclusion, we have seen that in all the cases treated here, the super-Poissonian value of  $F_2$  and the positive sign of  $F_{13}$  can be explained from the dynamical spin-blockade mechanism which induces a bunching of the tunneling events.

#### D. Effect of tunneling asymmetry

We now address the problem of how to choose parameters that favor the observation of positive cross-correlations in the ferromagnetic case treated here. First, from Section II C, finite lead polarizations are necessary. However, it is possible to get positive cross-correlations even if  $P_2 = 0$ , provided the output of the device is sufficiently polarized. For instance, in the high-voltage limit  $V = V_0^{\text{sgn}(E_0)}$ ; choosing  $P_1 = P_3$ ,  $P_2 = 0$  and  $\gamma_{sf} = 0$

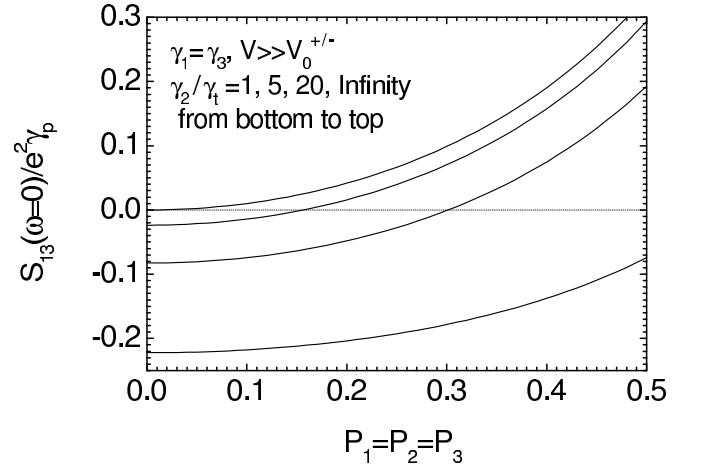


FIG. 10: Influence of the asymmetry between  $\gamma_2$  and  $\gamma_1$  on  $S_{13}(\omega=0)$ , for  $V = V_0^{\text{sgn}(E_0)}$ ,  $P_1 = P_3 = P_3$ ,  $\gamma_{sf} = 0$  and  $\gamma_1 = \gamma_3$ . According to (30),  $S_{13}(\omega=0)$  is always positive for high enough values of  $P_1$ . Large ratios  $\gamma_2 = e$  favor positive cross-correlations by extending the positivity domain to lower polarization values. In the limit  $\gamma_2 \rightarrow \infty$ , for  $P_1 = P_2 = P_3$ , one has  $S_{13}(\omega=0) = 4P_1^2P_3^2e^2 = t(1 - P_1^2)$  independent of  $\gamma_2$ . These high-voltage results are independent of the values of  $C_i$  considered.

leads to

$$S_{13}(\omega=0) = \frac{16e^2 \gamma_1^2 \gamma_3^2 (1 - P_1^2) (2\gamma_2 + t)}{t(2\gamma_2 + (1 - P_1^2)t)^3} \quad (29)$$

In this limit, the current  $hI_2i$  is not spin polarized, i.e.  $hI_{2,\uparrow}i = hI_{2,\downarrow}i$ , because up and down spins have the same probability to enter the dot, regardless of what happens at the output. The case where the three electrodes are polarized in the same direction leads to a higher positive  $S_{13}(\omega=0)$ . Indeed, in the high-voltage limit, choosing  $P_1 = P_2 = P_3$  and  $\gamma_{sf} = 0$  leads to

$$S_{13}(\omega=0) = \frac{16e^2 \gamma_1^2 \gamma_3^2 P_1^2 (2\gamma_2 + t)}{t(2\gamma_2 + t)^3 (1 - P_1^2)} \quad (30)$$

The asymmetry between the tunneling rates  $\gamma_i$  has a strong influence on the cross-correlations. From (30), the case of symmetric output junctions, i.e.  $\gamma_1 = \gamma_3$ ; is the most favorable configuration for getting a large  $S_{13}(\omega=0) > 0$  [42]. In addition, choosing large values of  $\gamma_2 = t$  decreases  $p_0$ , which allows to extend the domain of positive cross-correlations to smaller values of polarizations (Fig. 10). This is important because ferromagnetic materials are usually not fully polarized [43].

#### E. Finite frequency results

Equation (16) gives the frequency dependence of  $S_{13}(\omega)$ . The spectrum  $S_{13}(\omega)$  deviates from its zero frequency limit for  $\omega \neq j + j$ . In the case  $S_{13}(\omega=0) > 0$ ,

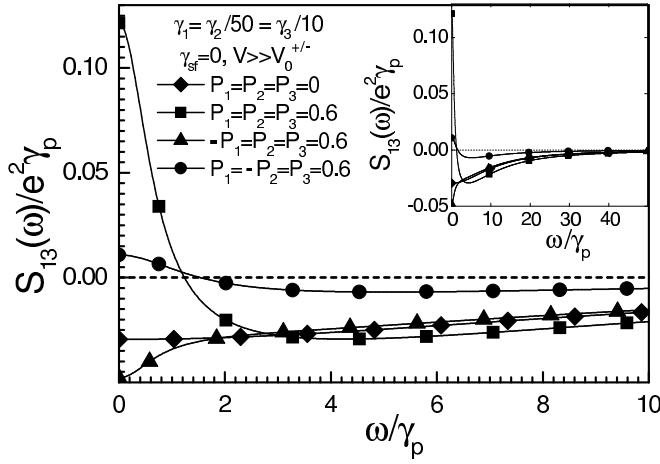


FIG. 11: Frequency dependence of  $S_{13}(\omega)$  in the high-voltage limit  $V \gg V_0^{\text{sgn}(\mathcal{E}_0)}$ , for the different cases considered in Figs. 2 to 7. The inset shows the same data for a larger frequency scale.

properties  $j + j < j - j$ ,  $C_{13}(t = 0) < 0$ ,  $S_{13}^+ > 0$  and  $S_{13}^- < 0$  (see Section II C) imply that cross-correlations always turn to negative when  $\omega$  increases. Then, for frequencies larger than  $j - j$ ,  $S_{13}(\omega)$  tends to zero (see Fig. 11).

Eq. (27) gives the expression of the total current cross-correlations  $S_{13}^{\text{tot}}(\omega)$  measured in practice, including the contribution of screening currents. The spectrum  $S_{13}^{\text{tot}}(\omega)$  differs from  $S_{13}(\omega)$  only for  $\omega < j + j$ . At large frequencies  $\omega \gg j - j$ ,  $S_{13}^{\text{tot}}(\omega)$  become a linear mixture of the Schottky noises through the three junctions. If we furthermore assume  $V \gg V_0^{\text{sgn}(\mathcal{E}_0)}$ , current conservation leads to

$$\frac{S_{13}^{\text{tot}}(\omega)}{2e} = \frac{I_1 C_3}{C^2} (C_1 - C_2 - C_3) + \frac{I_3 C_1}{C^2} (C_3 - C_1 - C_2).$$

This limit depends on the values of  $C_i$  considered, in contrast to what happens for  $S_{ij}(\omega)$ . It can be positive as well as negative depending on the values of parameters. For  $P_1 = P_2 = P_3 = 0.6$ ,  $\gamma_1 = \gamma_2 = \gamma_3 = 10$ ,  $C_1 = C_2 = C_3$  and  $V \gg V_0^{\text{sgn}(\mathcal{E}_0)}$ , one has a cross-over from positive to negative cross-correlations as  $\omega$  increases ( $S_{13}^{\text{tot}}(\omega = 0) = e^2 \gamma_p' + 0.121$  and  $S_{13}^{\text{tot}}(\omega \gg j - j) = e^2 \gamma_p' - 0.222$ ). But the opposite situation is also possible. For instance, with  $P_1 = P_2 = P_3 = 0$ ,  $\gamma_1 = \gamma_2 = \gamma_3 = 10$ ,  $C_1 = C_2 = C_3 = 5$  and  $V \gg V_0^{\text{sgn}(\mathcal{E}_0)}$ , one has  $S_{13}^{\text{tot}}(\omega = 0) = e^2 \gamma_p' - 0.030 < 0$  and  $S_{13}^{\text{tot}}(\omega \gg j - j) = e^2 \gamma_p' + 0.019 > 0$ . For other positive cross-correlations due to screening currents, see [25]. We recall that the results shown in this Section are valid if the Markovian approximation holds, i.e. here  $\omega \ll \min_i(\mathcal{E}_0 - eV_i)$  [38]. The results for the correlations of  $I_j^{\text{tot}}(t)$  are furthermore valid only for  $\omega$  larger than the characteristic frequencies associated to the charging of the capacitors (see Section

III E).

## F. Comments

In spite of the large variety of proposals for getting positive cross-correlations, this effect has not been observed experimentally yet. We believe that the mechanism proposed in Section III can be implemented with present techniques. For  $\gamma_1 = \gamma_2 = \gamma_3 = 10$ , the polarizations  $P_1 = P_2 = P_3 = 0.4$  typical for Co [43] lead to positive cross-correlations of the order of  $S_{13} = e^2 \gamma_{\text{tot}}' - 0.08$ . With  $\gamma_p' = 5$  GHz, this corresponds to a current noise level of  $10^{-29} \text{ A}^2 \text{ s}$ . The maximum differential conductance of the sample depends on temperature:  $dI_2/dV = e^2 \gamma_p (C_1 + C_3) = 5 k_B T C$ . Assuming that  $T = 20 \text{ mK}$  and  $C_1 = C_2 = C_3$ , one obtains  $(dI_2/dV)^{-1} = h/e^2$ . This leads to a voltage noise level measurable with existing voltage noise amplification techniques [29, 44].

One difficulty of this experiment is connecting three leads to a very small structure. We believe that a multiwall carbon nanotube (MWNT) contacted by ferromagnetic leads could be an interesting candidate for implementing a three-terminal device. The question of whether a MWNT splits into two quantum dots when three contacts are evaporated on top it is still open. However, given that the intrinsic level spacing of a MWNT connected to two leads seems to be determined by its total length rather than by the separation between the leads [45], a three-terminal quantum dot structure seems feasible. In addition, it has been demonstrated experimentally that contacting ferromagnetic leads to a MWNT is possible [46].

Interestingly, a different mechanism, proposed by Sauret and Feinberg, can also lead to positive current cross-correlations in a quantum-dot circuit [47]. This work also considers current transport through one single orbital of the dot. For certain bias voltages large enough to allow a double occupation of this orbital, the Pauli principle induces positive correlations between up and down spins. This so-called mechanism of "opposite-spin bunching" is antagonist to our mechanism of dynamical spin-blockade which requires that the orbital can be only singly occupied. However, with both mechanisms, positive cross-correlations can be obtained only when the two spin channels do not transport current independently, i.e. when charging effects are relevant [48]. We point out that in the three-terminal geometry of Figure (1), the opposite-spin bunching proposed by Sauret et al. allows to get positive output cross-correlations in spite of a sub-Poissonian input Fano factor. This feature, added to our findings, shows that positive output cross-correlations and a super-Poissonian input Fano factor can be obtained separately for a quantum dot connected to ferromagnetic leads. Nevertheless, the opposite-spin bunching proposed by Sauret et al. can lead to positive cross-correlations

between the total currents through leads 1 and 3 only when the output leads are strongly polarized in opposite directions, in order to filter the weak up-down positive cross-correlations induced by this effect. In practice, this is very difficult to achieve with usual ferromagnetic materials [43].

Note that the dynamical spin-blockade studied in this article is unrelated with another mechanism called "spin-blockade", observed in many semiconductor quantum dots experiments (see [49] and references therein). This other spin-blockade refers to the suppression of peaks expected in the I-V characteristics of a quantum dot for independent single electron states, but not observed due to quantum mechanical spin selection rules.

#### IV. ONE-ORBITAL QUANTUM DOT IN A MAGNETIC FIELD, CONNECTED TO THREE PARAMAGNETIC LEADS

In view of the experimental difficulties for connecting ferromagnetic leads to semiconductor quantum dots [50], the question of whether it is possible to obtain positive cross-correlations without using ferromagnetic leads is of great interest. We thus consider in Sections IV A and IV B the one-orbital case introduced in section II, with  $P_1 = P_2 = P_3 = 0$  and  $B \neq 0$ .

At  $B \neq 0$ , two resonances are expected a priori in the voltage characteristics, for  $V \sim V_{\text{m}}^{\text{sgn}(E_0)}$  and  $V \sim V_{\text{f}}^{\text{sgn}(E_0)}$ . The limit  $V \sim V_{\text{m}}^{\text{sgn}(E_0)}$  and  $\gamma_{\text{sf}} = 0$  is the same as in the  $B = 0$  case because the tunneling rates saturate at high voltages. In particular, from Eqs. (25), (28) and (30), we have in this limit

$$F_2 = \frac{4 \frac{t_2}{t} + \frac{t_2}{t}}{(t + 2 \frac{t_2}{t})^2} \quad (31)$$

$$F_{13} = \frac{4 \frac{t_1}{t} \frac{t_2}{t} \frac{t_3}{t}}{t (t + 2 \frac{t_2}{t})^2}.$$

This means that here, a super-Poissonian  $F_2$  and positive cross-correlations can appear only at lower voltages, for which the cases  $E_0 > 0$  and  $E_0 < 0$  differ significantly. Note that due to  $P_1 = P_2 = P_3 = 0$ , one obtains from Eqs. (4) and (12):

$$S_{13} = \frac{1}{t} \frac{t_3}{t} F \left( \frac{t_2}{t}; \frac{t_{\text{f}}}{t}; \frac{t_{\text{f}}}{t}; \frac{E_0}{T}; \frac{V}{T}; \frac{B}{T} \right) \quad (32)$$

According to (32), for a constant value of  $t$ ,  $t_1 = t_3$  allows to maximize  $|S_{13}|$ . Therefore, in this section, we will plot curves for  $t_1 = t_3$ .

##### A. Zero-frequency results for $E_0 > 0$

We first briefly comment the case in which the two Zeeman sublevels are above the Fermi energy at equilib-

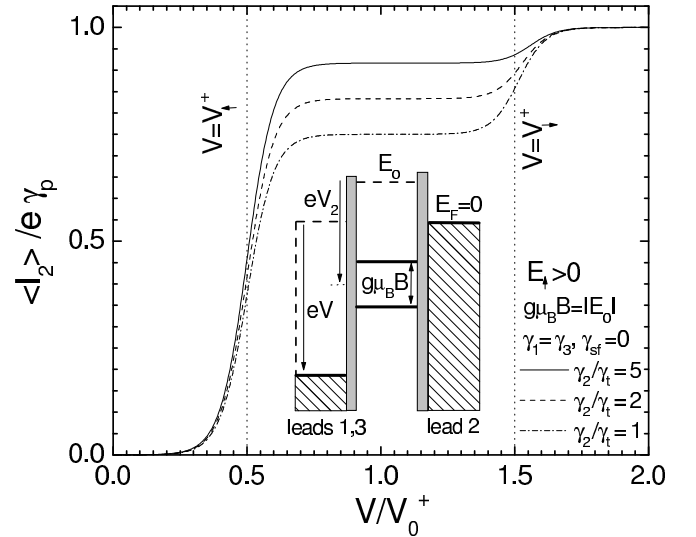


FIG. 12: Average current  $\langle I_2 \rangle$  as a function of the bias voltage  $V$  for  $E_0 > 0$ ,  $P_1 = P_2 = P_3 = 0$ ,  $C_1 = C_2 = C_3$ ,  $t_1 = t_3$ ,  $k_B T = \hbar \omega_j = 0.05$ ,  $g \mu_B B = \hbar \omega_j = 1$ , and different values of  $\gamma_2 = t$ . These curves display two steps, for  $V \sim V_{\text{m}}^+$  and  $V \sim V_{\text{f}}^+$ . The inset shows electrochemical potentials in the circuit.

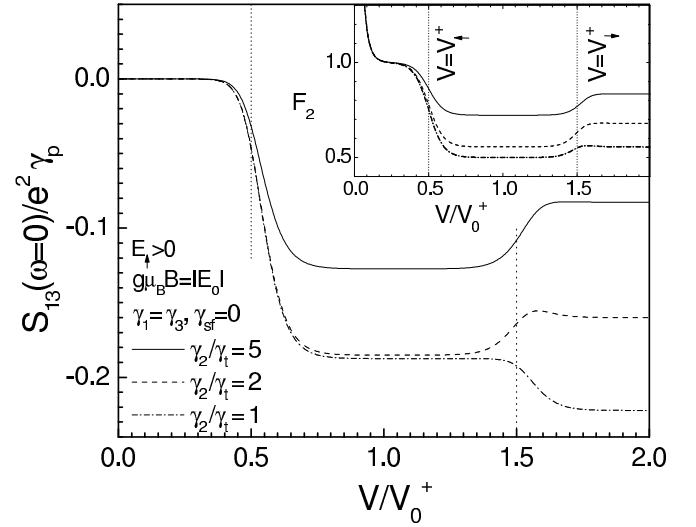


FIG. 13: Zero-frequency current cross-correlations  $S_{13} (! = 0)$  between leads 1 and 3 as a function of the bias voltage  $V$  for the same circuit parameters as in Fig. 12. Inset: Fano factor  $F_2$ . These curves display two steps, for  $V \sim V_{\text{m}}^+$  and  $V \sim V_{\text{f}}^+$ . Above the thermal peak, for  $\gamma_{\text{sf}} = 0$ , one has  $F_2 \rightarrow 1$  and  $S_{13} (! = 0) \rightarrow 0$  for any values of the parameters.

rium (i. e.  $E_{\text{f}}(\#) > 0$ ). The current and noise voltage-characteristics obtained in this situation were already discussed in Ref. [51] for the two-terminal case. Like in IIIA, for  $V < V_{\text{m}}^+$ ,  $\langle I_2 \rangle$  and  $S_{13} (! = 0)$  are exponentially small and  $F_2$  is Poissonian with a thermal peak at  $V \sim 0$ , followed by a unitary plateau (Figs. 12 and 13). Then, the curves  $\langle I_2 \rangle$ ;  $F_2$  and  $S_{13} (! = 0)$  show two steps corresponding to  $V \sim V_{\text{m}}^+$  and then  $V \sim V_{\text{f}}^+$ . We

have verified analytically that, above the thermal peak, for  $\gamma_{sf} = 0$ , one has  $F_2 \rightarrow 1$  and  $F_{13} \rightarrow 0$  for any values of the parameters. For  $V < V_{\#}^+$ , the current  $\langle I_2 \rangle$  is spin polarized, an effect which allows to do spin filtering with a nearly 100% efficiency [52, 53].

B. Zero-frequency results for  $E_0 < 0$

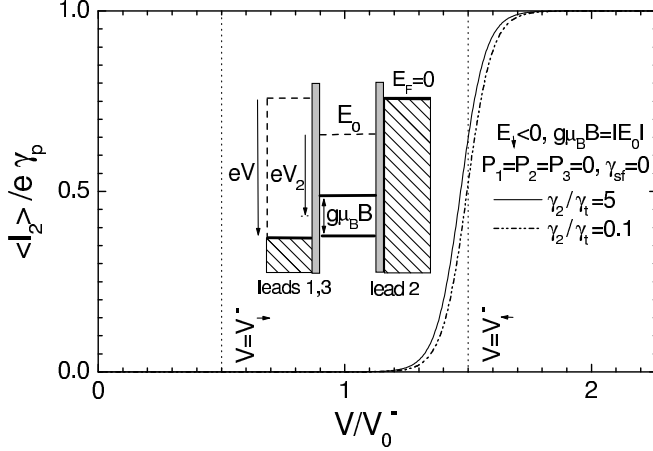


FIG. 14: Current-voltage characteristic of the circuit of Fig. 1 for  $E_0 < 0$ ,  $P_1 = P_2 = P_3 = 0$ ,  $C_1 = C_2 = C_3$ ,  $\gamma_1 = \gamma_3$ ,  $k_B T = \beta_0 j = 0.05$ ,  $g_B B = \beta_0 j = 1$ , and different values of the asymmetry  $\gamma_2 = \gamma_t$  between the input and the output. These curves display only one step, for  $V > V_{\#}^+$ . The inset shows the electrochemical potentials in the circuit.

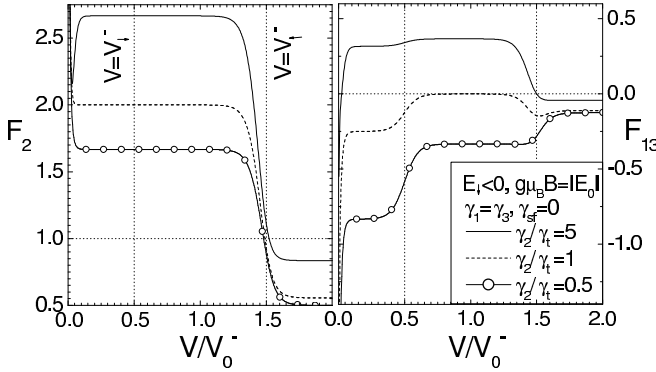


FIG. 15: Input Fano factor  $F_2$  (left panel) and output cross-Fano factor  $F_{13}$  (right panel) as a function of the bias voltage  $V$ , for the same circuit parameters as in Fig. 14. In all curves  $\gamma_{sf} = 0$ :  $F_2$  can be super-Poissonian and  $F_{13}$  positive for certain values of  $\gamma_2 = \gamma_t$  (see text). The Fano factor  $F_2$  shows only one step for  $V > V_{\#}^+$ , whereas  $F_{13}$  shows two steps, for  $V > V_{\#}^+$  and  $V > V_{\#}^+$ .

Below, we focus on the case in which the two Zeeman sublevels are below the Fermi energy at equilibrium (i.e.  $E_{\#(\pm)} < 0$ ). To our knowledge, the current noise in this configuration has never been studied

before, even for a two-terminal device. We will first study analytically what happens above the thermal peak, i.e.  $eV > k_B T$ . In this limit, one can write the tunneling rates as  $\gamma_2^+ = \gamma_2$ ,  $\gamma_2^- = 0$ ,  $\gamma_{1(3)}^+ = x \gamma_{1(3)}$ ,  $\gamma_{1(3)}^- = (1-x) \gamma_{1(3)}$ ,  $\gamma_{1(3)\#}^+ = y \gamma_{1(3)}$ , and  $\gamma_{1(3)\#}^- = (1-y) \gamma_{1(3)}$ , where  $x = 1/(1 + \exp[(E_{\#} - eV_1)/k_B T])$  and  $y = 1/(1 + \exp[(E_{\#} - eV_1)/k_B T])$ . The hypothesis  $B > 0$  implies that  $x < y$ . First, for  $V < V_{\#}^+$ ; we have  $x \rightarrow 0$  and  $y \rightarrow 0$ . Then, the parameters  $x$  and  $y$  go from 0 to 1 while the voltage increases. For  $V = V_{\#}^+$  i.e.  $y = 1/2$ , the upper Zeeman sublevel is at resonance with the Fermi level of the output leads 1 and 3. Then, for  $V = V_{\#}^+$  i.e.  $x = 1/2$ , the lower Zeeman sublevel is at resonance with the outputs, as represented by the level diagram in Fig. 14.

The assumptions made on the rates lead to

$$F_{13} = \frac{1}{2} \frac{3}{2} \left[ \gamma_2 (F_2 - 1) + \gamma_t (x + y - 2) \right]. \quad (33)$$

In Section II, we have shown that relation (25) between  $F_2$  and  $F_{13}$  is always valid at high voltages (i.e.  $x, y \rightarrow 1$  here) for the single-orbital problem with  $P_1 = P_2 = P_3$ . But this demonstration does not take into account the symmetries that the problem takes for certain particular cases. Here, from (33),  $P_1 = P_2 = P_3 = 0$  implies that property (25) is also valid at any  $V$  above the thermal peak when  $\gamma_2 = \gamma_t$ .

The inequality  $\gamma_{\#} = 1 - \gamma_t \neq \gamma_t = 1 - x$  for  $x \neq y$  suggests the possibility of obtaining again dynamical spin-blockade. To study the situation accurately, we will consider the simplified situation  $k_B T \ll g_B B$ , i.e. the up-spins channel starts to conduct for voltages such that down spin can flow only from the right to the left. This means that for the first voltage transition  $V > V_{\#}^+$ , we have  $x \rightarrow 1$  and it is enough to consider low order developments of  $\langle I_2 \rangle$ ,  $F_2$ , and  $F_{13}$  with respect to  $x$ :

$$\langle I_2 \rangle = \frac{2e \gamma_2 \gamma_t x}{\gamma_2 + \gamma_t} + o(x)^2, \quad (34)$$

$$F_2 = \frac{\gamma_t + 3 \gamma_2}{\gamma_2 + \gamma_t} + o(x) \quad (35)$$

and

$$F_{13} = \frac{1}{2} \frac{3}{2} \left( \frac{\gamma_2^2}{\gamma_2 + \gamma_t} - \gamma_t \frac{(1 + \gamma_2)}{2 \gamma_t} \right) + o(x) \quad (36)$$

for  $\gamma_{sf} = 0$ . Transport through the upper level is energetically allowed for  $y > 1/2$ . However, since we have assumed  $x \rightarrow 1$ , from Eq. (34),  $\langle I_2 \rangle$  remains very small throughout the  $V > V_{\#}^+$  transition: the dot is blocked by up spins, thus down spins cannot cross the dot. Even if the current is very low, this leads to dynamical spin-blockade and thus to a super-Poissonian  $F_2$ , except in the limit  $\gamma_t \rightarrow \gamma_2$  [see Eq. (35)]. Accordingly,  $F_{13}$  can

be positive for certain tunneling rate asymmetries [Eq. (36)]. The factor  $F_{13}$  shows a step around  $V \sim V_\#$ , due to the  $y$  dependence in Eq. (36), whereas  $F_2$  is constant throughout the  $V \sim V_\#$  transition. This implies a redistribution of the zero-frequency noise between  $S_{11}$  ( $! = 0$ ),  $S_{33}$  ( $! = 0$ ) and  $S_{13}$  ( $! = 0$ ) when the threshold  $V = V_\#$  is crossed [see (23)]. The absence of step for  $F_2$  can be attributed to the unidirectionality of tunneling through junction 2. Indeed,  $x \neq 0$  means that  $F_2$  depends only on  $p_0$  and  $G_{0,\#}$  [see (7) and (12)]. Now, for  $V \sim V_\#$ ; the contribution of these terms is independent of  $y$  (and thus on  $V$ ) at first order in  $x$ , because  $p_0$  and  $G_{0,\#}$  are already forced to very low values due to the  $x \neq 0$  hypothesis. On the contrary,  $F_{13}$  also depends on  $p_\#$  and  $G_{\#0}$  with  $2 \ll \#; 0g$ . For  $x \neq 0$ , these last terms depend strongly on  $y$ .

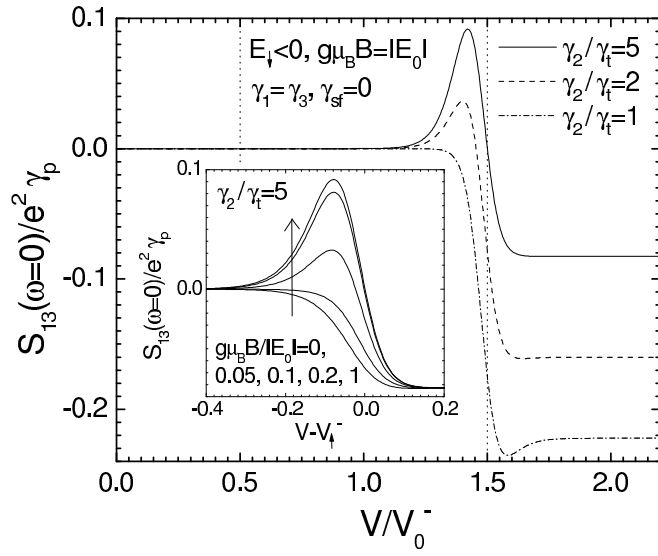


FIG. 16: Zero-frequency current cross-correlations  $S_{13}(! = 0)$  between leads 1 and 3 as a function of the bias voltage  $V$ , for the same circuit parameters as in Fig. 14 and different values of junction asymmetry. The inset shows the effect of a magnetic field  $B$  for  $\gamma_2 = \gamma_1 = 5$  and  $\gamma_{sf} = 0$ .

For  $k_B T \ll g_B B$ , the second possible voltage transition  $V \sim V_\#$  can be described by taking the limit  $y = 1$  where

$$hI_2 i = \frac{2ex_2 t}{t + 2(1+x)}, \quad (37)$$

$$F_2 = 1 + \frac{2x_2 t(1 - 3x) + (1 - x^2)_2}{(t + 2(1+x))^2} \quad (38)$$

and

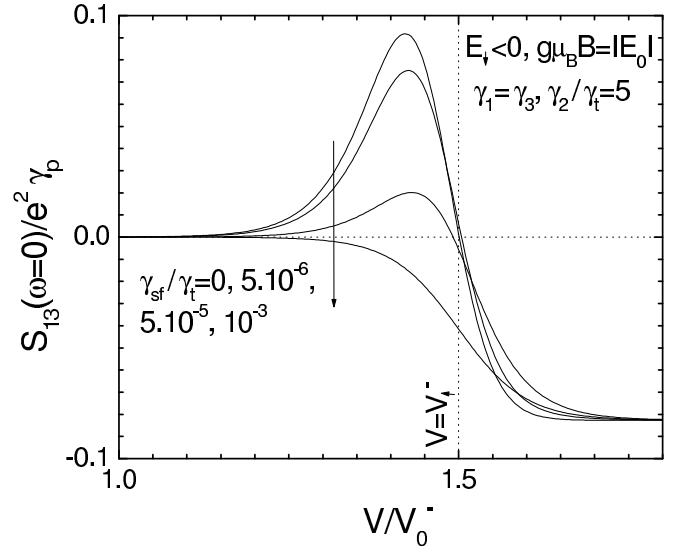


FIG. 17: Effect of spin flip-scattering on the current cross-correlations between leads 1 and 3 for the same circuit parameters as in Fig. 16 and  $\gamma_2 = \gamma_1 = 5$ .

$$F_{13} = \frac{1}{2} \frac{3}{t} \frac{1}{2(t + (1+x)_2)^2} \left[ \frac{2(1 - x^2)_2^3 + (1 - 7x + x^2 + x^3)_2^2 t}{2(1 - x^2)_2^2 (1 - x)_t^3} \right] \quad (39)$$

for  $\gamma_{sf} = 0$ . Around  $V \sim V_\#$ , the blockade of the dot by up spins is partially lifted and transport through both levels is allowed. The average input current  $hI_2 i$  thus increases with voltage (i.e. with  $x$ ) [see (37)]. On the opposite of what happens in IV A, the average current  $hI_2 i$  is not spin-polarized because up and down spin have the same probability to enter the dot. The factors  $F_2$  and  $F_{13}$  both show a step through the  $V \sim V_\#$  transition (as indicated by their  $x$ -dependency) and tend at high voltages to the usual sub-Poissonian values.

We now turn to the discussion of the general results displayed in Figs. (14-17), obtained from an exact treatment of the full Master equation. Fig. 14 shows the full voltage dependence of  $hI_2 i$ . As expected from (34) and (37), this current shows a single step at  $V \sim V_\#$ , an effect observed experimentally [54, 55, 56]. The width on which  $hI_2 i$  varies is of the order of  $V \sim 10k_B T C = eC_2$ , whereas the position of the step varies only slightly with the asymmetry of the junctions (the maximal variation is about  $V \sim 0.7k_B T C = eC_2$ ).

The left panel of Fig. 15 shows the voltage dependence of  $F_2$ . The divergence  $2k_B T = eV$  of  $F_2$  at zero voltage is again a result of the dominating thermal noise in the limit  $k_B T > eV$ . As expected from (35) and (38),  $F_2$  shows one single step at  $V \sim V_\#$ , which is super-Poissonian except for  $t \rightarrow 2$ . The right panel of Fig. 15 shows the

voltage dependence of  $F_{13}$ . As expected,  $F_{13}$  shows two steps at  $V' = V_{\#}$  and then  $V' = V_{\#}$ . The first plateau is positive for  $\gamma_2 > \gamma_1 + \frac{1}{5} = 2$  and the second for  $\gamma_2 > \gamma_1$ , as can be seen from (36). The high-voltage plateau is negative as usual. The case  $\gamma_2 = \gamma_1 = 1=2$  and  $V_{\#} < V < V_{\#}$  is one more illustration that it is possible to have  $F_2$  super-Poissonian and  $F_{13} < 0$ .

It is also interesting to look at  $S_{13}(! = 0)$  which is the signal measured in practice (Fig. 16). Like  $hI_2$ , the cross-correlations  $S_{13}(! = 0)$  are exponentially small for  $V' = V_{\#}$ , thus the first voltage step of  $F_{13}$  is not visible on the scale of Fig. 16. Cross-correlations have a significant variation around  $V' = V_{\#}$ , with a positive peak for  $\gamma_2 > \gamma_1$ . The maximum positive  $S_{13}(! = 0)$  obtained at this peak is of the same order as the maximum  $S_{13}(! = 0)$  predicted in the ferromagnetic case for comparable junction asymmetries (see Section III F). Note that the height of the positive peak is independent of temperature as long as (1) is fulfilled, whereas its width, which is approximately  $V_{\#}$ , depends on temperature.

Since the positive cross-correlations found in this work are due to dynamical spin-blockade, we expect a strong dependence on the magnetic field. The inset of Fig. 16 shows the voltage dependence of  $S_{13}(! = 0)$  around the step  $V_{\#}$ , for a fixed temperature, a tunneling asymmetry  $\gamma_2 = \gamma_1 = 5$ ; and various magnetic fields. The amplitude of the positive peak first increases with  $B$  and then saturates once the Zeeman splitting of the levels is much larger than the thermal smearing of the resonances (i.e.  $g_B B \gg 8k_B T$ ). The peak then simply shifts to larger voltages while  $B$  increases. Fig. 17 shows the effect of spin- $\uparrow\downarrow$  scattering on the cross-correlations. Spin- $\uparrow\downarrow$  modify the positive peak of  $S_{13}(! = 0)$  when  $\gamma_{\#} = \gamma_{sf} \exp(g_B B / 2k_B T)$ , see Eq. (4). It is thus preferable to use a  $B$  not larger than  $8k_B T$  when spin- $\uparrow\downarrow$  scattering is critical. As expected, a strong spin- $\uparrow\downarrow$  scattering suppresses all spin-effects and turns the positive cross-correlations to negative.

### C. Comments

There is a strong qualitative difference between the ferromagnetic case of Section III and the  $B \neq 0$  case of Section IV: in Section IV we have obtained positive cross-correlations in the form of a peak around a resonance voltage whereas in Section III, positive cross-correlations reach their maximum above the resonance voltage.

In practice, we can imagine to tune the bias voltage  $V$  such that different orbital levels will transport current successively while the gate voltage of the dot is swept, leading to an effective  $E_0$  oscillating between positive and negative values. In this situation, the results of Sections IV A and V B indicate the possibility of having the sign of  $S_{13}(! = 0)$  which oscillates with the gate voltage.

MWNTs could be possible candidates for observing

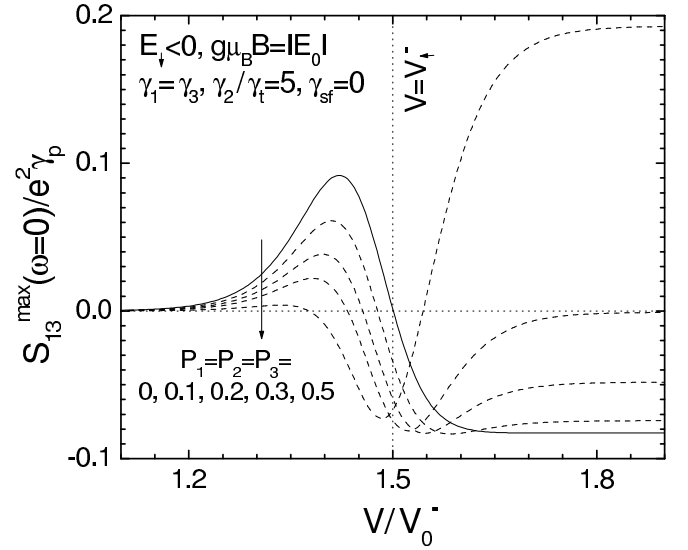


FIG. 18: Zero-frequency current cross-correlations between leads 1 and 3 as a function of the bias voltage for the same circuit parameters as in Fig. 16,  $\gamma_2 = \gamma_1 = 5$  and  $\gamma_{sf} = 0$ . The full line corresponds to the case  $P_1 = P_2 = P_3 = 0$  shown in Fig. 16 and the dashed lines to finite values of  $P_1 = P_2 = P_3$ .

this effect. However, lateral semiconductor quantum dots seem even more attractive. The fabrication technology of lateral semiconductor quantum dots allows to engineer more than two leads just by adjusting a lithography pattern (see for instance [39]). Another advantage of these structures is that the asymmetry of the tunnel junctions, which is very critical for getting dynamical spin-blockade, can be controlled just by changing the voltage of the gates delimiting them. In addition, it has been shown that the spin- $\uparrow\downarrow$  rate can be very low in semiconductor quantum dots [56, 57]. However, implementing the model of Section IV requires that the leads can be considered as unpolarized, which is not obvious in these systems if the magnetic field is not applied locally to the dot but to the whole circuit. In certain cases, the magnetic field can induce a significant spin polarization at the edges of the two-dimensional electron gas, leading to different net tunneling rates  $j_{\uparrow\#}$  and  $j_{\downarrow\#}$  for up and down spins [53, 58, 59]. In an extremely simplified approach, we have taken this effect into account with finite polarizations  $P_1 = P_2 = P_3$  with the same sign as  $B$  (see Fig. 18). The positive peak of  $S_{13}(! = 0)$  is suppressed while  $P_1$  increases because the tunneling rates of spins which blocked the dot for  $P_1 = P_2 = P_3 = 0$  increase. However, this positive peak is replaced by a high-voltage positive limit simply identical to that of Section III for the corresponding polarizations. Note that for semiconductor quantum dots in the few electron regime, the time evolution of  $j_{\text{dot}}$  can be measured by coupling the dot to a single electron transistor or a quantum point contact [60, 61, 62, 63]. In the high-voltage limit where cur-

rent transport is unidirectional, studying the statistics of  $j_{\text{dot}}(t)j_{\text{w}}(t)$  would give a direct access to  $S_{22}(!)$  for currents too low to be measured with standard techniques.

## V. TWO-ORBITAL SPIN-DEGENERATE QUANTUM DOT CIRCUIT

### A. Mapping onto the one-orbital non spin-degenerate case

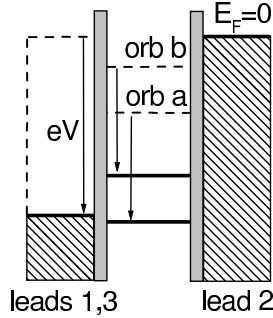


FIG. 19: Electrochemical potentials for a quantum dot connected to three paramagnetic leads and subject to no magnetic field, with two different orbitals levels a and b accessible for current transport.

We now consider the quantum dot circuit of Fig. 1 with  $V > 0$ , connected to paramagnetic leads ( $P_1 = P_2 = P_3 = 0$ ) and with no magnetic field ( $B = 0$ ). We assume that two different orbitals levels a and b of the dot are accessible for current transport, but we still consider that the dot cannot be doubly occupied. We define  $j_{j\text{orb}}$  as the net tunneling rate between lead j and the orbital orb 2 fa;bg. This problem is spin-degenerate and can thus be treated without the spin degree of freedom, which is replaced by the orbital degree of freedom. The rate for an electron to tunnel between lead j and the orbital level orb in direction is  $j_{j\text{orb}} = j_{j\text{orb}}(1 + \exp[(E_{\text{orb}} - eV_j)/k_B T])$ , where  $E_{\text{orb}}$  is the intrinsic energy of the orbital level orb. This problem can be treated in the sequential tunneling limit with a Master equation analog to (3). There is in fact a direct mapping between this problem and that described in Section II. We will assume that  $E_a < E_b$ , so that the orbitals a and b will play the roles of the Zeeman sub-levels " and # of Section II, where  $B > 0$ . One has to replace the parameters of the previous problem by

$$\begin{aligned} E_{\text{"}(\text{"})} & \rightarrow E_{a(b)}, \\ j_j & \rightarrow \frac{j_{ja} + j_{jb}}{2}, \\ P_j & \rightarrow P_j = \frac{j_{ja} - j_{jb}}{j_{ja} + j_{jb}}, \\ \text{"}(\text{"}) & \rightarrow ab(ba). \end{aligned} \quad (40)$$

This mapping shows that one can obtain positive cross-correlations in this two-orbital system. It provides the evidence that interactions can lead to zero-frequency positive cross-correlations in a normal quantum dot circuit even without lifting spin-degeneracy. Note that in practice,  $j_{ja} = j_{jb}$  is not obvious because of the different spatial extensions of the orbitals (see for instance [39, 53]). This problem is thus equivalent to a one-orbital problem with  $B \neq 0$  and with finite effective polarizations  $P_1, P_2, P_3$  which can be close to  $\pm 1$ . Positive cross-correlations can be expected either at the resonance associated to level b (for  $E_b < 0$ ) or in the plateau following this resonance, depending on the parameters (see for instance Fig. 18).

### B. Comments

In the one-orbital ferromagnetic case, we have shown that the simple relation (25) between  $F_2$  and  $F_{13}$  is valid in the high-voltage limit only when  $P_1 = P_3$ . Therefore, according to the mapping indicated in Section V A., in the two-orbital case, relation (25) is valid in the high-voltage limit only if  $P_1 = P_3$  i.e.  $j_{1a} = j_{3a} = j_{1b} = j_{3b}$ . Hence, the range of validity of property (25) found in Section IID for the one-orbital system cannot be generalized to the two-orbital case.

In the spin-degenerate case treated here, positive cross-correlations stem from the partial blockade of an electronic channel by another one, thus we suggest to call this effect: dynamical channel blockade. This effect should be observable in semiconductor quantum dots. The advantage of taking  $B = 0$  is that the problem of spurious lead polarization evoked in Section IV is suppressed. When  $eV \gg E_b + E_C$  and  $s_f = 0$ , the two channels conduct current independently, thus dynamical channel blockade is suppressed and the positive cross-correlations disappear (see (40) + [48]). When  $E \ll k_B T$ , cross-correlations are always negative in a spin-degenerate three-terminal quantum dot placed in the sequential tunneling limit [28]. Therefore, the hypothesis  $E \ll k_B T$  is also necessary to obtain positive cross-correlations in this device. In fact, when  $E \ll k_B T$ , the electron leaving the dot at a given time is not necessarily the one which entered the dot just before, in spite of  $eV \gg E_C$ : channel effects are suppressed.

Note that a super-Poissonian Fano factor can also be obtained in a spin-degenerate circuit based on two biternal quantum dots (or localized impurity states) placed in parallel and coupled electrostatically to each other [64, 65, 66]. If one of the dots is charged, the other cannot transport current because of the Coulomb repulsion. The dot which changes its occupancy with a slower rate modulates the current through the other one, which leads to a dynamical channel blockade analogous to what we found. The possibility to get positive cross-



correlations in these systems was not investigated, but Section V of the present article suggests it.

## V I. C O N C L U S I O N

We have considered noise in a three-terminal quantum dot operated as a beam splitter. In this system, a super-Poissonian input Fano factor is not equivalent to zero-frequency positive output cross-correlations. We have studied three different ways to get these two effects, due to the mechanism of dynamical channel blockade. The first two strategies consist in involving only one orbital of the dot in the electronic transport and lifting spin-degeneracy, either by using ferromagnetic leads or by applying a magnetic field to the dot. We have furthermore shown that lifting spin degeneracy is not necessary anymore when two orbitals of the dot are involved in the current transport. These results show that one can get zero-frequency positive cross-correlations due to interactions inside a beam splitter circuit, even if this is a spin-degenerate normal fermionic circuit with a perfect voltage-bias.

We thank H. A. Engel, K. Ensslin, M. Governale, H. Grabert, R. Hanson, T. Kontos, R. Leturcq, B. Reulet, I. Sa, P. Samuelsson and B. Trauzettel for interesting discussions. We are particularly indebted to M. Buttiker for raising the question which led us to consider the case treated in Section V. This work was financially supported by the RTN Spintronics, by the Swiss NSF and the NCCR Nanoscience.

- 
- [1] Ya. M. Blanter and M. Buttiker, Phys. Rep. 336, 1 (2000).
  - [2] Quantum Noise in Mesoscopic Physics, edited by Yu. V. Nazarov (Kluwer, Dordrecht, 2003).
  - [3] V. A. Khlus, Sov. Phys. JETP 66, 1243 (1987).
  - [4] G. B. Lesovik, JETP Lett. 49, 592 (1989).
  - [5] M. Buttiker, Phys. Rev. Lett. 65, 2901 (1990).
  - [6] M. Buttiker, Phys. Rev. B 46, 12485 (1992).
  - [7] M. Henny, S. Oberholzer, C. Strunk, T. Heinzel, K. Ensslin, M. Holland, and C. Schonenberger, Science 284, 296 (1999).
  - [8] W. D. Oliver, J. Kin, R. C. Liu, and Y. Yamamoto, Science 284, 299 (1999).
  - [9] S. Oberholzer, M. Henny, C. Strunk, C. Schonenberger, T. Heinzel, K. Ensslin, and M. Holland, Physica E 6, 314 (2000).
  - [10] See the article of M. Buttiker, in Ref. [2].
  - [11] T. Martin, Phys. Lett. A 220, 137 (1996).
  - [12] M. P. A. Nantram, and S. Datta, Phys. Rev. B 53, 16390 (1996).
  - [13] J. Torres and T. Martin, Eur. Phys. J. B 12, 319 (1999).
  - [14] T. Gramschpacher and M. Buttiker, Phys. Rev. B 61, 8125 (2000).
  - [15] J. Torres, T. Martin, and G. B. Lesovik, Phys. Rev. B 63, 134517 (2001).
  - [16] M. Shechter, Y. Imry, and Y. Levinson, Phys. Rev. B 64, 224513 (2001).
  - [17] J. Borlin, W. Belzig, and C. Bruder, Phys. Rev. Lett. 88, 197001 (2002).
  - [18] P. Samuelsson and M. Buttiker, Phys. Rev. Lett. 89, 046601 (2002).
  - [19] P. Samuelsson and M. Buttiker, Phys. Rev. B 66, 201306 (2002).
  - [20] F. Taddei and R. Fazio, Phys. Rev. B 65, 134522 (2002).
  - [21] D. Sanchez, R. Lopez, P. Samuelsson, and M. Buttiker, Phys. Rev. B 68, 214501 (2003).
  - [22] G. Bignon, M. Houzet, F. Pistolesi, and F. W. J. Hekking, cond-mat/0310349.
  - [23] C. Texier and M. Buttiker, Phys. Rev. B 62, 7454 (2000).
  - [24] M. Gattobigio, G. Iannaccone, and M. M. acucci Phys. Rev. B 65, 115337 (2002).
  - [25] A. M. Martin and M. Buttiker, Phys. Rev. Lett. 84, 3386 (2000).
  - [26] I. Sa, P. Devillard, and T. Martin, Phys. Rev. Lett. 86, 4628 (2001).
  - [27] A. N. Korotkov, Phys. Rev. B 49, 10381 (1994); S. Hershfeld, J. H. Davies, P. Hyldgaard, C. J. Stanton, and J. W. Wilkins, ibid. 47, 1967 (1993); U. Hanke, Yu. M. Galperin, K. A. Chao, and N. Zou, ibid. 48, 17209 (1993).
  - [28] D. A. Bagrets and Yu. V. Nazarov, Phys. Rev. B 67, 085316 (2003).
  - [29] H. Birk, M. J. M. de Jong, and C. Schonenberger, Phys. Rev. Lett. 75, 1610 (1995); H. Birk, K. Oostveen, and C. Schonenberger, Rev. Sci. Instrum. 67, 2977 (1996).
  - [30] B. R. Bulka, J. Martinek, G. M. Chakraborty, and J. Bamas, Phys. Rev. B 60, 12246 (1999); B. R. Bulka, Phys. Rev. B 62, 1186 (2000).
  - [31] E. V. Sukhomukov, G. Burkard, and D. Loss, Phys. Rev. B 63, 125315 (2001).
  - [32] D. V. Averin, in Macroscopic Quantum Coherence and Quantum Computing, edited by D. V. Averin, B. Ruggerio, and P. Silvestrini (Kluwer, Dordrecht, 2001); cond-mat/0010052.
  - [33] F. Yamaguchi, and K. Kawamura, Physica (Amsterdam) 227B, 116 (1996); G. H. Ding and T. K. Ng, Phys. Rev. B 56, R15521 (1997); Y. Meir and A. Golub, Phys. Rev. Lett. 88, 116802 (2002).
  - [34] A. Cottet, W. Belzig, and C. Bruder, cond-mat/0308564, to be published in Phys. Rev. Lett.
  - [35] A. Cottet and W. Belzig, cond-mat/0401456, to be published in Europhys. Lett.
  - [36] W. Belzig and M. Zareyan, cond-mat/0307070.
  - [37] M. Julliere, Phys. Lett. A 54, 225 (1975).
  - [38] H. A. Engel and D. Loss, cond-mat/0312107.
  - [39] R. Leturcq, D. Graf, T. Ihn, K. Ensslin, D. Driscoll, and A. C. Gossard (unpublished).
  - [40] M. M. Deshmukh, and D. C. Ralph, Phys. Rev. Lett. 89, 266803 (2002); M. M. Deshmukh, E. Bonet, A. N. Pasupathy, and D. C. Ralph, Phys. Rev. B 65, 073301 (2002).
  - [41] Note that  $n_b = I_2 = I_2^\#$  includes bunches with no up spins, i.e. two down spins passing consecutively. Thus,  $n_b$  can be smaller than 1.
  - [42] Note that despite this, we have chosen to show in Sections II A and II B curves for the case  $s_3 = s_1 = 10$  because it allows to get, just by reversing the polarization of one output lead, both the cases where  $S_{13} (= 0)$  is positive or negative while  $F_2$  is super-Poissonian.

- [43] R. J. Soulen Jr., J. M. Byers, M. S. Osofsky, B. N. Adgomy, T. Ambrose, S. F. Cheng, P. R. Broussard, C. T. Tanaka, J. Nowak, J. S. Moodera, A. Barry, and J. M. D. Coey, *Science* 282, 85 (1998).
- [44] D. C. Glatli, P. Jacques, A. Kumar, P. Pari, and L. Saminadayar, *J. Appl. Phys.* 81, 7350 (1997).
- [45] M. R. Buitelaar, A. Bachtold, T. Nussbaumer, M. Iqbal, and C. Schonenberger, *Phys. Rev. Lett.* 88, 156801 (2002).
- [46] K. Tsukagoshi, B. W. Alphenaar, and H. Ago, *Nature* 401, 572 (1999).
- [47] O. Sauret and D. Feinberg, *Phys. Rev. Lett.* 92, 106601 (2004).
- [48] In the one-orbital case, positive cross-correlations can be obtained only if the tunneling rates for one spin direction depend on the occupation of the other spin level. When charging effects are not relevant, i.e.  $V_{\text{eff}} + E_C j_C = (C_1 + C_3)$  for  $E_0 > 0$  or  $V_{\text{eff}} + E_C j_C = C_2$  for  $E_0 < 0$ , the tunneling rates become independent of the occupation of the dot. We have verified analytically (calculation not shown here) that in these conditions, for  $s_f = 0$ ,  $S_{13} (! = 0)$  is always negative for any polarization of the leads 1, 2, 3 and any spin- $\uparrow$  rate.
- [49] A. K. Huttel, H. Qin, A. W. Holleitner, R. H. Blick, K. Neumaier, D. Weinmann, K. Eberl, and J. P. Kotthaus, *Europhys. Lett.* 62, 712 (2003).
- [50] G. Schmidt, D. Ferrand, L. W. Molenkamp, A. T. Filip, and B. J. van Wees, *Phys. Rev. B* 62, R4790 (2000); A. Khaetskii, J. C. Egues, D. Loss, C. Gould, G. Schmidt, and L. W. Molenkamp, *cond-mat/0312705*.
- [51] A. Thielenmann, M. H. Hettler, J. König, and G. Schon, *Phys. Rev. B* 68, 115105 (2003).
- [52] P. Recher, E. V. Sukhorukov, and D. Loss, *Phys. Rev. Lett.* 85, 1962 (2000).
- [53] R. Hanson, L. M. K. Vandersypen, L. H. Willem van Beveren, J. M. Elzerman, I. T. Vink, and L. P. Kouwenhoven, *cond-mat/0311414*.
- [54] D. C. Ralph, C. T. Black, and M. Tinkham, *Phys. Rev. Lett.* 74, 3241 (1995); *ibid.* 78, 4087 (1997).
- [55] D. H. Cobden, M. Bockrath, P. L. McEuen, A. G. Rinzier, and R. E. Smalley, *Phys. Rev. Lett.* 81, 681 (1998); D. H. Cobden and J. Nygard, *ibid.* 89, 046803 (2002).
- [56] R. Hanson, B. Witkamp, L. M. K. Vandersypen, L. H. Willem van Beveren, J. M. Elzerman, and L. P. Kouwenhoven, *Phys. Rev. Lett.* 91, 196802 (2003).
- [57] A. V. Khaetskii and Yu. V. Nazarov, *Phys. Rev. B* 61, 12639 (2000); *ibid.* 64, 125316 (2001); S. I. Erlingsson and Yu. V. Nazarov *ibid.* 66, 155327 (2002).
- [58] M. Ciorga, M. Pioro-Ladrière, P. Zawadzki, P. Hawrylak, and A. S. Sachrajda, *Appl. Phys. Lett.* 80, 2177 (2002).
- [59] M. C. Rogge, C. Fühner, U. F. Keyser, and R. J. Haug, *cond-mat/0310469*.
- [60] W. Lu, Z. Ji, L. Pfeiffer, K. W. West, and A. J. Rimberg, *Nature* 423, 422 (2003).
- [61] M. Field, C. G. Smith, M. Pepper, D. A. Ritchie, J. E. F. Frost, G. A. C. Jones, and D. G. Hasko, *Phys. Rev. Lett.* 70, 1311 (1993).
- [62] J. M. Elzerman, R. Hanson, J. S. Greidanus, L. H. Willem van Beveren, S. De Franceschi, L. M. K. Vandersypen, S. Tarucha, and L. P. Kouwenhoven, *Phys. Rev. B* 67, 161308(R) (2003).
- [63] R. Schleser, E. Ruh, T. Ihn, K. Ensslin, D. C. Driscoll, and A. C. Gossard (unpublished).
- [64] S. S. Safonov, A. K. Savchenko, D. A. Bagrets, O. N. Jouravlev, Y. V. Nazarov, E. H. Linfeld, and D. A. Ritchie, *Phys. Rev. Lett.* 91, 136801 (2003).
- [65] G. Kießlich, A. Wacker, and E. Scholl, *Phys. Rev. B* 68, 125320 (2003).
- [66] A. Nauen, F. Hohls, J. Königmann, and R. J. Haug, *cond-mat/0402358*.